

Nonperturbative renormalization of composite operators with overlap fermions

J.B. Zhang¹, N. Mathur^{2,3}, S.J. Dong², T. Draper², I. Horváth²,
F.X. Lee³, D.B. Leinweber¹, K.F. Liu², and A.G. Williams¹

¹ *Special Research Center for the Subatomic Structure of Matter and Department of Physics
University of Adelaide, Adelaide, SA 5005, Australia*

² *Department of Physics and Astronomy,*

University of Kentucky, Lexington, KY 40506

³*Jefferson Lab, 12000 Jefferson Avenue, Newport News, VA 23606 and*

⁴*Center for Nuclear Studies, Department of Physics,
George Washington University, Washington, DC 20052*

Abstract

We compute non-perturbatively the renormalization constants of composite operators on a quenched $16^3 \times 28$ lattice with lattice spacing $a = 0.20$ fm for the overlap fermion by using the regularization independent (RI) scheme. The quenched gauge configurations were generated with the Iwasaki action. We test the relations $Z_A = Z_V$ and $Z_S = Z_P$ and find that they agree well (less than 1%) above $\mu = 1.6$ GeV. We also perform a Renormalization Group (RG) analysis at the next-to-next-to-leading order and match the renormalization constants to the $\overline{\text{MS}}$ scheme. The wave-function renormalization Z_ψ is determined from the vertex function of the axial current and Z_A from the chiral Ward identity. Finally, we examine the finite ma corrections for the renormalization factors of the quark bilinear operators. We find that the $(pa)^2$ errors of the vertex functions and the $m\Lambda_{QCD}a^2$ and $(ma)^2$ corrections of the renormalization factors are small.

PACS numbers: 12.38.Gc, 11.15.Ha, 12.38.Aw,

I. INTRODUCTION

Lattice QCD is a unique tool to compute the mass spectrum, leptonic decay constants and hadronic matrix elements of local operators non-perturbatively from first principles. Renormalization of lattice operators is an essential ingredient needed to deduce physical results from numerical simulations. In this paper we study the renormalization properties of composite bilinear operators with the overlap quark action.

In principle, renormalization of quark bilinears can be computed by lattice perturbation theory. However, lattice perturbation theory converges slowly and the expansion parameter, the square of the lattice coupling evaluated at the lattice scale, $g_0(a)^2$, decreases only as an inverse power of $\ln(a)$, hence the higher-order corrections may not be small, thus introducing a large uncertainty in the calculation of the renormalized matrix elements in some continuum scheme. In general, it is difficult to go beyond one loop in such calculations. To overcome these difficulties, Martinelli *et al.* [1] have proposed a promising non-perturbative renormalization procedure. The procedure allows a full non-perturbative computation of the matrix elements of composite operators in the Regularization Independent (RI) scheme [1, 2]. The matching between the RI scheme and $\overline{\text{MS}}$, which is intrinsically perturbative, is computed using only the well behaved continuum perturbation theory.

This method has been shown to be quite successful in reproducing results obtained by other methods, such as chiral Ward Identities [3]. The method has also been successfully applied to determine renormalization coefficients for various operators using the Wilson [4, 5, 6, 7] and staggered actions [8], domain-wall fermions [9], chirally improved fermions [10], as well as the quark mass renormalization constant for overlap fermions [11]. The purpose of the current work is to study the application of this non-perturbative renormalization procedure to the renormalization of the quark field and the flavor non-singlet fermion bilinear operators, and also to study their ma dependence for the case of overlap fermions.

Neuberger's overlap fermion [12, 13] is shown to have correct anomaly and exact chiral symmetry on the lattice [12, 13, 14] with finite cut-off. As a consequence, many chiral-symmetry relations [14, 15] and the quark propagator [16] preserve the same structure as in the continuum. The use of the overlap action entails many theoretical advantages [17]: it has no additive mass renormalization, there are no order- a artifacts, and it has good scaling behavior with small $O(a^2)$ and $O(m^2a^2)$ errors [16, 18]. In addition, it forbids mixing

among operators of different chirality and, therefore, it can be very helpful in computing weak matrix elements.

The outline of this paper is as follows. In Sec. II, we review the non-perturbative method (NPM) proposed in Ref. [1] and introduce the notation used in the remainder of this work. In Sec. III, we briefly describe the overlap fermion formalism. We present the numerical results for the renormalization constants as well as the Renormalization Group (RG) analysis of the quark bilinear in Sec. IV and Sec. V. In Sec. VI, we examine the finite ma behavior of the renormalization factors of the quark bilinear operators. We complete our discussion with our conclusions in Sec. VII.

II. NON-PERTURBATIVE RENORMALIZATION METHOD

In this section, we review the nonperturbative renormalization method of Ref. [1], which we will use to compute the renormalization constants of quark bilinears in this paper. The method imposes renormalization conditions non-perturbatively, directly on quark and gluon Green's functions in Landau gauge.

We start by considering the definition for the momentum space quark propagator. Let $S(x, 0)$ be the quark propagator on the gauge-fixed configuration from a source 0 to all space-time points x . The momentum space propagator is defined as the discrete Fourier transform over the sink positions

$$S(p, 0) = \sum_x \exp(-ip^{\text{latt}} \cdot x) S(x, 0), \quad (1)$$

where p^{latt} the dimensionless lattice momenta

In our case, we use the periodic boundary condition in spatial directions and the anti-periodic boundary condition in time direction. We have then the dimensionful momenta

$$p_i = \frac{2\pi}{N_s a}(n_i - N_i/2), \quad \text{and} \quad p_t = \frac{2\pi}{N_t a}(n_t - 1/2 - N_t/2), \quad (2)$$

for an $N_s^3 \times N_t$ lattice.

We also define the square of the absolute momentum as the Euclidean inner product of the momentum defined in Eq. (??) or Eq. (2)

$$(pa)^2 = \sum_{\mu} p_{\mu}^{\text{latt}} p_{\mu}^{\text{latt}}, \quad (3)$$

where we use convention that p is dimensionful and p_{μ}^{latt} is dimensionless.

A. Three Point Function

Consider the fermion bilinear operator

$$O_\Gamma(x) = \bar{\psi}(x)\Gamma\psi, \quad (4)$$

where Γ is the Dirac gamma matrix

$$\Gamma \in \{1, \gamma_\mu, \gamma_5, \gamma_\mu\gamma_5, \sigma_{\mu\nu}\} , \quad (5)$$

and the corresponding notation will be $\{S, V, P, A, T\}$ respectively. The three point function with the operator insertion at position 0 and the propagator from y to 0 and then from 0 to x is given by

$$G_O(x, 0, y) = \langle \psi(x)O_\Gamma(0)\bar{\psi}(y) \rangle = \langle S(x, 0)\Gamma S(0, y) \rangle, \quad (6)$$

where $S(0, y)$ is the quark propagator from y to 0. It is the inverse of the Dirac operator [48]. Note, $S(x, 0)$ here is not translational invariant. Only when averaging over all gauge configurations, i.e.,

$$\langle S(x, 0) \rangle, \quad (7)$$

is it translational invariant.

The Fourier transform of the three-point function is given by

$$\begin{aligned} G_O(pa, p'a) &\equiv \int d^4x d^4y e^{-i(p \cdot x - p' \cdot y)} G_O(x, 0, y), \\ &= \langle \left(\int d^4x S(x, 0) e^{-ip \cdot x} \right) \Gamma \left(\int d^4y S(0, y) e^{ip' \cdot y} \right) \rangle, \\ &= \langle S(p, 0) \Gamma \gamma_5 \left(\int d^4y S^\dagger(y, 0) e^{ip' \cdot y} \right) \gamma_5 \rangle, \end{aligned} \quad (8)$$

where the \dagger refers only to the color and spin indices. This can be written as

$$G_O(pa, p'a) = \langle S(p, 0) \Gamma (\gamma_5 S^\dagger(p', 0) \gamma_5) \rangle, \quad (9)$$

From this, one can define the amputated three-point function

$$\Lambda_O(pa, p'a) = S(pa)^{-1} G_O(pa, p'a) S(p'a)^{-1}, \quad (10)$$

where

$$S(pa) = \langle S(p, 0) \rangle \quad (11)$$

which is translational invariant and is a 12×12 matrix.

Finally, a projected vertex function is defined

$$\Gamma_O(pa) = \frac{1}{\text{Tr}(\hat{P}_O^2)} \text{Tr} \left(\Lambda_O(pa, pa) \hat{P}_O \right), \quad (12)$$

where $\hat{P}_O = \Gamma$ is the corresponding projection operator.

B. RI-MOM Renormalization Condition

The renormalized operator $O(\mu)$ is related to the bare operator

$$O(\mu) = Z_O(\mu a, g(a)) O(a), \quad (13)$$

and the renormalization condition is imposed on the three-point vertex function $\Gamma_O(pa)$ at a scale $p^2 = \mu^2$ as

$$\Gamma_{O,\text{ren}}(pa)|_{p^2=\mu^2} = \frac{Z_O(\mu a, g(a))}{Z_\psi(\mu a, g(a))} \Gamma_O(pa)|_{p^2=\mu^2} = 1 \quad (14)$$

to make it agree with the tree-level value of unity [1]. Here Z_ψ is the field or wave-function renormalization

$$\psi_{\text{ren}} = Z_\psi^{1/2} \psi. \quad (15)$$

This gives a well-defined procedure for the RI renormalization at the scale μ . In practice, one frequently needs to match to the perturbative scheme, e.g. $\overline{\text{MS}}$ scheme, to compare with experimental quantities. We will discuss perturbative matching in Sec. IV. In general, the vertex function $\Gamma_O(pa)$ may have intrinsically non-perturbative contributions, e.g. from the Goldstone boson propagator, which are not included in perturbative calculations. To this end, we either go to large enough momentum such that the non-perturbative effects are suppressed or somehow remove them from the data.

In order to obtain the renormalization constant Z_O for the operator O , one needs to know Z_ψ first. There are several ways to obtain it. The first suggestion is to extract Z_ψ from the vertex function for the conserved vector or axial-vector current. For example, if one uses the conserved vector current, then $Z_{V_C} = 1$. From the renormalization condition

$$\frac{Z_{V_C}}{Z_\psi} \Gamma_{V_C}(pa)|_{p^2=\mu^2} = 1, \quad (16)$$

one then obtains

$$Z_\psi = \frac{1}{48} \text{Tr} (\Lambda_{V_{C\mu}}(pa) \gamma_\mu) |_{p^2=\mu^2}. \quad (17)$$

One can also extract Z_ψ directly from the quark propagator. From Ward Identity (WI), it follows [1]

$$Z_\psi = \frac{-i}{12} \text{Tr} \left[\frac{\partial S(pa)^{-1}}{\partial p} \right]_{p^2=\mu^2}. \quad (18)$$

To avoid derivatives with respect to a discrete variable, it is suggested [1] to use

$$Z'_\psi = \frac{-i}{12} \frac{\text{Tr} \sum_{\mu=1}^4 \gamma_\mu (p_\mu a) S(pa)^{-1}}{4 \sum_{\mu=1}^4 (p_\mu a)^2} \Bigg|_{p^2=\mu^2}, \quad (19)$$

which, in the Landau gauge, differs from Z_ψ by a finite term of order α_s^2 [19]. The matching coefficient can be computed using continuum perturbation theory, and up to order α_s^2 [19]

$$\frac{Z'_\psi}{Z_\psi} = 1 - \frac{\alpha_s^2}{(4\pi)^2} \Delta_\psi^{(2)} + \dots \quad (20)$$

In the Landau gauge

$$\Delta_\psi^{(2)} = \frac{(N_c^2 - 1)}{16 N_c^2} (3 + 22N_c^2 - 4N_c n_f), \quad (21)$$

where N_c is the number of colors and n_f the number of dynamical quarks. However, as pointed in Ref. [9], due to the ambiguity of how the discrete lattice momentum p is defined, this method will introduce roughly 10% – 20% uncertainty.

The third way to get Z_ψ is to calculate the renormalization constant Z_A from the axial Ward identity [20] with a local current, and then use it to extract Z_ψ from the vertex function Γ_A . Note here, the local axial-vector current is finite. Thus, Z_A is independent of scale, but depends on the lattice spacing a . We expect it (and the Z_V of the local vector current) to go to unity at the continuum limit. In this case, the renormalization condition

$$\frac{Z_A}{Z_\psi} \Gamma_A(pa) |_{p^2=\mu^2} = 1, \quad (22)$$

gives

$$Z_\psi = \frac{Z_A}{48} \text{Tr} (\Lambda_{A_\mu}(pa) \gamma_\mu \gamma_5) |_{p^2=\mu^2}. \quad (23)$$

Once Z_ψ is secured, one can use it to calculate other renormalization constants, such as Z_S , Z_P , Z_V , and Z_T and check the identity relations $Z_S = Z_P$ and $Z_V = Z_A$ due to chiral symmetry.

In this work, we shall adopt the third approach as mentioned above. It is known that Z_A determined from the Ward identity has a small statistical error at the level of 0.2% [20] and will not contribute much to the overall error. When we study the finite ma dependence, we shall extract the finite ma dependence of the wave-function renormalization from the quark propagator in order to obtain the finite ma errors for the renormalization factors of the quark bilinear operators.

III. OVERLAP FERMION

The massless overlap-Dirac operator in dimensionless lattice units is [13]

$$D(0) = [1 + \gamma_5 \epsilon(H)] , \quad (24)$$

where $\epsilon(H)$ is the matrix sign function of an Hermitian operator H . $\epsilon(H)$ depends on the background gauge field and has eigenvalues ± 1 . Any such D is easily seen to satisfy the Ginsparg–Wilson relation [21]

$$\{\gamma_5, D\} = D\gamma_5 D . \quad (25)$$

It follows easily that $\{\gamma_5, D^{-1}(0)\} = \gamma_5$ and by defining $\tilde{D}^{-1}(0) \equiv [D^{-1}(0) - 1/2]$ we see that it anticommutes with γ_5

$$\{\gamma_5, \tilde{D}^{-1}(0)\} = 0 . \quad (26)$$

The standard choice of $\epsilon(H)(x, y)$ is $\epsilon(H) \equiv H_W/|H_W| = H_W/(H_W^\dagger H_W)^{1/2}$, where $H_W(x, y) = \gamma_5 D_W(x, y)$ is the Hermitian Wilson-Dirac operator. D_W is the usual Wilson-Dirac operator on the lattice. However, in the overlap formalism the Wilson mass parameter ρ need to be negative in order to generate zero modes.

In the present work, we use the standard Wilson-Dirac operator, which can be written as

$$D_W(x, y) = \left[\delta_{x,y} - \kappa \sum_{\mu} \left\{ (r - \gamma_{\mu}) U_{\mu}(x) \delta_{y,x+\hat{\mu}} + (r + \gamma_{\mu}) U_{\mu}^\dagger(x - a\hat{\mu}) \delta_{y,x-\hat{\mu}} \right\} \right] . \quad (27)$$

The negative Wilson mass $-\rho$ is then related to κ by

$$\kappa \equiv \frac{1}{2(-\rho) + 8} . \quad (28)$$

ρ is chosen such that $\kappa > \kappa_c$ and $\rho < 2r$, and hence there is no species doubling and there are zero modes for the massless quark. In this work, $r = 1$ and $\rho = 1.368$ (which corresponds to $\kappa = 0.19$) in our numerical simulation.

It is shown that the flavor non-singlet scalar, pseudo-scalar [22], vector, and axial [22, 23] bilinears in the form $\bar{\psi}KT(1 - \frac{1}{2}D)\psi$ (K is the kernel which includes γ matrices and T is the flavor $SU(N_f)$ matrix) transform covariantly under the global chiral transformation $\delta\psi = T\gamma_5(1 - D/2)\psi$ as in the continuum. The $1 - \frac{1}{2}D$ factor is also understood as the lattice regulator which projects out the unphysical real eigenmodes of D at $\lambda = 2$. For the massive case, the fermion action is defined as $\bar{\psi}\rho D\psi + ma\bar{\psi}(1 - \frac{1}{2}D)\psi$ so that the tree-level wave-function renormalization of the quark propagator is unity. In this case, the Dirac operator can be written as

$$D(m) = \rho D + ma(1 - \frac{1}{2}D) = \rho + \frac{m}{2} + (\rho - \frac{m}{2})\gamma_5\epsilon(H). \quad (29)$$

With the ψ field in the operators and the interpolation fields for hadrons replaced by the lattice regulated field $\hat{\psi} = (1 - \frac{1}{2}D)\psi$, the regulator factor will be associated with the quark propagator in the combination $(1 - \frac{1}{2}D)D(m)^{-1}$ in Green's functions, leading to an effective quark propagator [16]

$$S(x, y) = (1 - \frac{1}{2}D)D(m)^{-1} = (D_c + m)^{-1}. \quad (30)$$

where the operator $D_c = \rho D/(1 - \frac{1}{2}D)$ is chirally symmetric in the continuum sense, i.e. $\{\gamma_5, D_c\} = 0$ [24, 25]; but, unlike D , it is non-local. The effective quark propagator in Eq. (30) turns out to be the same as simply adding the mass term m to the D_c in the propagator [26, 27, 28]. It is stressed [16] that the effective quark propagator has the continuum form, i.e. the inverse propagator is the sum of a chirally symmetric Dirac operator and a mass parameter. The mass in the quark propagator is the same bare mass m in the fermion action. Thus the massive overlap fermion can be used to study both light quarks and heavy quarks. The only question is how large the $O(ma^2)$ and $O(m^2a^2)$ errors are [16].

IV. NUMERICAL RESULTS

In this paper we work on a $16^3 \times 28$ lattice with lattice spacing, $a=0.20$ fm, as determined from the pion decay constant f_π [29]. The gauge configurations are created by the Iwasaki

gauge action through the pseudo-heat-bath algorithm. A total of 80 configurations are used. The lattice parameters are summarized in Table I.

TABLE I: Lattice parameters.

Action	Volume	N_{Therm}	N_{Samp}	β	a (fm)	Physical Volume (fm ⁴)
Iwasaki	$16^3 \times 28$	10000	5000	2.264	0.200	$3.2^3 \times 5.60$

The gauge field configurations are gauge fixed to the Landau gauge using a Conjugate Gradient Fourier Acceleration [30] algorithm with an accuracy of $\theta \equiv \sum |\partial_\mu A_\mu(x)|^2 < 10^{-12}$. We use an improved gauge-fixing scheme [31] to minimize gauge-fixing discretization errors.

Our numerical calculation begins with an evaluation of the inverse of $D(m)$ which is defined in Eq. (29). We use a 14th order Zolotarev approximation [32] to the matrix sign function $\epsilon(H_W)$. In the selected window of $x \in [0.031, 2.5]$ of $\epsilon(x)$, the approximation is better than 3.3×10^{-10} [29]. We then calculate Eq. (30) for each configuration by using multi-mass Conjugate Gradient method for both the inner and outer loops. The detailed numerical description is given in Ref. [29]. In the calculations, $\kappa = 0.19$ was used, which corresponds to $\rho = 1.368$. We calculate 15 quark masses by using a shifted version of the Conjugate Gradient solver [15, 18]. The bare quark masses ma are chosen to be $ma = 0.2100, 0.03033, 0.04433, 0.06417, 0.07583, 0.08983, 0.10850, 0.12950, 0.15633, 0.18783, 0.22633, 0.26833, 0.32200, 0.40000$, and 0.60000 . With the scale determined by f_π , they correspond to pion masses $212(7), 247(6), 290(6), 342(6), 370(7), 400(7), 438(7), 478(8), 524(8), 575(9), 633(10), 692(11), 764(12), 862(13), 1092(17)$ MeV respectively [29].

In the following, we give the steps for the numerical calculation:

- After we calculate the quark propagators in coordinate space for each configuration, we use the Landau gauge fixing transformation matrix to rotate the quark propagators to the Landau gauge. The discrete Fourier transformation is then used to calculate the quark propagators in momentum space.
- Next, we calculate the five projected vertex functions $\Gamma_O(pa)$ defined in Eq. (12), where we have used the effective quark propagator in Eq. (30) for the calculation. By definition, they are the ratios of the renormalization constants at the chiral limit (i.e. $Z_\psi(\mu a, g(a))/Z_O(\mu a, g(a))$ from Eq. (14)) in the RI scheme at scale $\mu^2 = p^2$. They are

in general dependent on $(pa)^2$ and this dependence comes from two sources. One is from the running of the renormalization constants in the RI scheme, the other is from the possible $(pa)^2$ error.

- We decouple the two above mentioned scale dependences of the calculated $\Gamma_O(pa)$ by first dividing out its perturbative running in the RI scheme. Ideally, this should take care of the scale dependence, since we have taken the scale to infinity. However, due to the $(pa)^2$ error on the lattice, there can still be some $(pa)^2$ dependence in the $\Gamma_O(pa)$ after undoing the perturbative running. Following Ref. [9], we shall attribute the remaining scale dependence to the $(pa)^2$ error and will use the simple linear fit to remove it. This will be discussed in Section V. For the scalar and pseudo-scalar vertex functions, there is an additional complication due to the presence of quark mass poles [9]. We shall remove them first and then extrapolate to the chiral limit. Finally, we can check the expected relations $Z_A = Z_V$ and $Z_S = Z_P$.
- In order to compare results with experiments, one frequently quotes the scale-dependent results in the $\overline{\text{MS}}$ scheme at certain scale. So the final step is to perturbatively match the results from the RI scheme to the $\overline{\text{MS}}$ scheme at $\mu = 2 \text{ GeV}$ for Z_S , Z_P , and Z_T .

A. Axial and vector currents

Let us consider first the vector and axial vector currents. Since each obeys a Ward Identity [33], their renormalization constants are finite. In Fig. 1, we show the vertex functions Γ_A and Γ_V from Eq. (12) for different bare quark masses as a function of the lattice momentum $(pa)^2$. We find that they are weakly dependent on the mass, and almost scale independent after $(pa)^2 \geq 2.0$, which corresponds to $p \geq 1.4 \text{ GeV}$.

In the RI scheme, Eq. (14) implies that in the chiral limit

$$\lim_{m \rightarrow 0} \Gamma_{A/V}(pa)|_{p^2=\mu^2} = Z_\psi(\mu a, g(a))/Z_{A/V}, \quad (31)$$

and one expects that $Z_A = Z_V$ for the overlap fermion, but this is true only for large momenta p . At low momenta, Γ_A and Γ_V may differ due to the effects of spontaneous chiral symmetry breaking [9].

Following Ref. [9], we show in Fig. 2 the quantities $\Gamma_A - \Gamma_V$ and $\frac{1}{2}(\Gamma_A + \Gamma_V)$, after linearly extrapolating with respect to ma to the chiral limit. We can observe from the

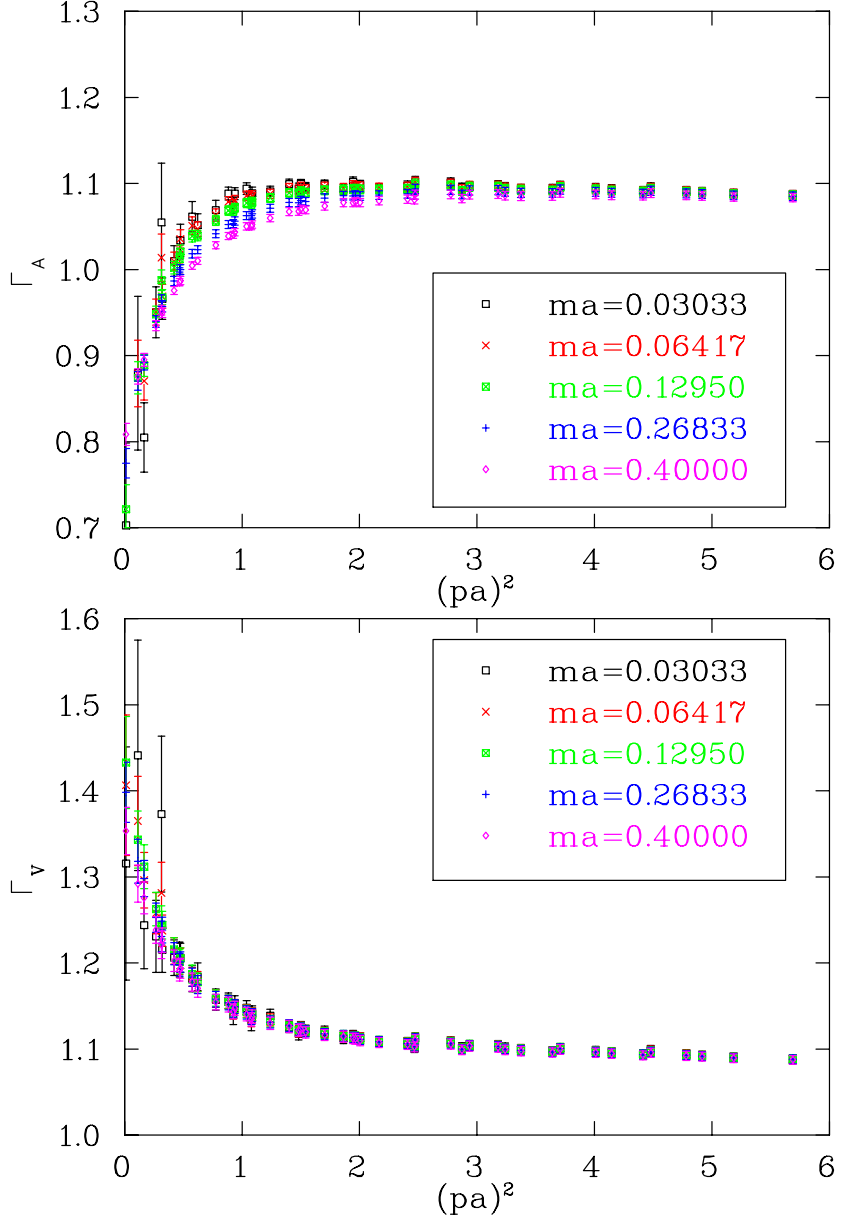


FIG. 1: The projected vertex function Γ defined in Eq. (12) for the vector and axial-vector currents with different bare quark masses.

upper panel of the figure that there is no effect of spontaneous chiral symmetry breaking at moderate and high momenta, where $\Gamma_A - \Gamma_V$ tends to zero. In fact, the percentage error between Γ_A and Γ_V is less than 1% at $(ap)^2 = 2.5$ (top panel) and is comparable to the statistical error. This deviation is further smaller for higher momenta. On the other hand, the effects of spontaneous chiral symmetry breaking are clearly visible at low momenta where Γ_A and Γ_V differ. In the lower panel of Fig. 2, we plot $\frac{1}{2}(\Gamma_A + \Gamma_V)$ against $(pa)^2$. Since Z_V and Z_A are scale independent, the slight $(pa)^2$ dependence that one observes in $\frac{1}{2}(\Gamma_A + \Gamma_V)$

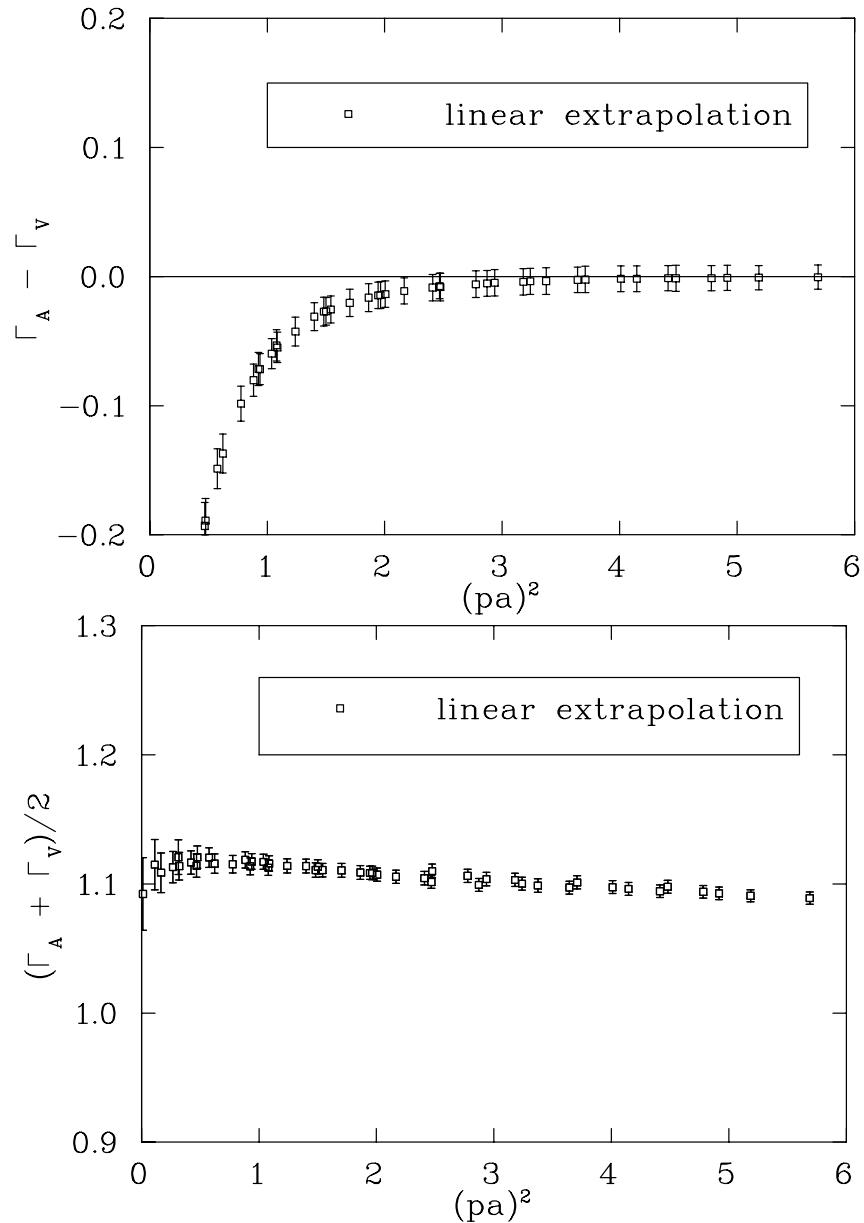


FIG. 2: The upper panel is $(\Gamma_A - \Gamma_V)$ versus $(pa)^2$. We see that $Z_A = Z_V$ is valid above moderate $(pa)^2 \sim 2.5$. Here we linear extrapolate to the chiral limit ($m = 0$) with ma . The lower one is $\frac{1}{2}(\Gamma_A + \Gamma_V)$ versus $(pa)^2$.

in Fig. 2 for $(pa)^2 > 2.5$ reflects the scale dependence of Z_ψ and the lattice $(pa)^2$ error.

B. Pseudo-scalar and scalar densities

The pseudo-scalar and scalar densities differ from the axial and vector currents as their renormalization constants are not scale independent. For massless overlap fermions, the

scalar and pseudo-scalar currents with the form $\bar{\psi}(1 - D/2)\psi$ and $\bar{\gamma}_5\psi(1 - D/2)\psi$ transform as the continuum under the lattice chiral transformation [14, 34, 35]. From the Ward identities, one obtains the relations

$$Z_S = Z_P \quad (32)$$

$$Z_m = \frac{1}{Z_S}. \quad (33)$$

Thus, the quantities Z_S/Z_P , $Z_S Z_m$ and $Z_m Z_P$ are expected to be scale independent.

For the case of the pseudo-scalar and scalar renormalization, there is a complication due to the presence of the quark condensate in the inverse quark propagator. Using the axial Ward identity from the quark propagator, one has [9]

$$m\Gamma_P(p, p) = \frac{1}{12}Tr(S^{-1}(p)). \quad (34)$$

It is known that due to the spontaneous chiral symmetry breaking, the trace of the inverse quark propagator picks up a contribution from the quark condensate [36]. At large p^2 [36], it is given by

$$\frac{1}{12}Tr(S^{-1}(p)) = m - \langle \bar{q}q \rangle \frac{4\pi\alpha_s}{3p^2} + O(1/p^4). \quad (35)$$

from first order perturbation [36]. This implies that the renormalized $Tr(S_{ren}^{-1}(p))$ should be

$$\frac{1}{12}Tr(S_{ren}^{-1}(p)) = m_{ren} - C_1 \frac{\langle \bar{q}q \rangle}{p^2} + O(1/p^4). \quad (36)$$

In the study of lattice artifacts of the Wilson fermion [37], it is shown that there are three terms which mix at $O(a)$ to give an improved and renormalized quark field,

$$q_{ren} = Z_\psi^{1/2}(1 + b_q ma)\{1 + ac'_q(\not{D} + m_{ren}) + ac_{NGI} \not{\partial}\}q_0, \quad (37)$$

where $\not{\partial}$ may appear due to gauge fixing. It is found [37] in the study of the order $O(a)$ error of Wilson fermion, that c'_q is large. Combining Eqs. (36) and (37), one has [9]

$$\frac{1}{12}Tr(S_{latt}^{-1}(pa)) = \dots + Z_m Z_\psi(ma + m_{res}a) - C_1 Z_\psi \frac{a^3 \langle \bar{q}q \rangle}{(pa)^2} + 2(c_{NGI} - c'_q)(pa)^2 + O(1/p^4), \quad (38)$$

where terms of $O(m c_{NGI})$ are neglected. Thus, in this case, $\frac{1}{12}Tr(S_{latt}^{-1}(pa))$ diverges for large pa .

On the other hand, it is learned from the domain wall fermion [9] study on a $16^3 \times 32 \times 16$ lattice with Wilson gauge action at $\beta = 6.0$, the explicit chiral symmetry breaking effect

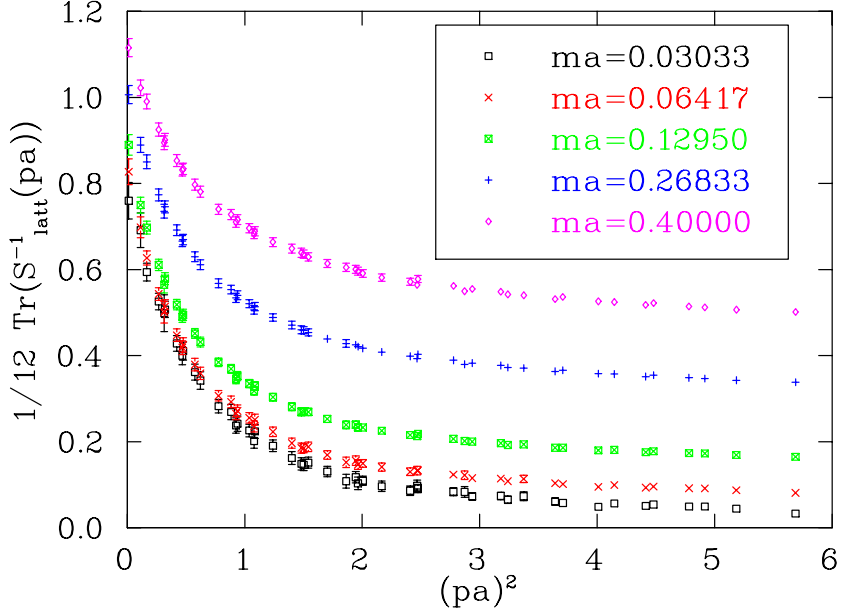


FIG. 3: A plot of $\frac{1}{12}Tr(S_{latt}^{-1}(pa))$ versus $(pa)^2$ for different bare quark mass ma on $16^3 \times 28$ lattice, showing that $\frac{1}{12}Tr(S_{latt}^{-1}(pa))$ approaches a constant value at large $(pa)^2$.

from the $c_{NGI} - c'_q$ term is negligible for moderately large values of $(pa)^2$ and that the residual mass is small. Since the explicit symmetry breaking is controlled to a level $< 10^{-9}$ with the Zoloterav approximation of the sign function [29] for the overlap fermion, we expect the $c_{NGI} - c'_q$ term to be negligibly small. It was already shown that the residual quark mass due to the numerical approximation of the overlap operator is negligible [18]. Here, we shall verify the expectation that the $c_{NGI} - c'_q$ term is negligible.

As shown in Fig. 3, $\frac{1}{12}Tr(S_{latt}^{-1}(pa))$ for several quark masses tend to constant values after $(pa)^2 \geq 4$. This indicates that there is no discernible contamination due to the explicit chiral symmetry term $2(c_{NGI} - c'_q)(pa)^2$ which grows as $(pa)^2$. Fig. 4 shows the same at the chiral limit which is obtained from linear extrapolation in ma . In this case, $\frac{1}{12}Tr(S_{latt}^{-1}(pa))$ tends to zero at large $(pa)^2$ as expected from Eq. (38) with no residual mass. Plotted in Fig. 5 is the slope of $\frac{1}{12}Tr(S_{latt}^{-1}(pa))$ with respect to the quark mass ma . It is expected to be $Z_m Z_\psi$ at large $(pa)^2$ from Eq. (38). These results are very similar to those of the domain wall fermion [9].

From Eqs. (34) and (38), one finds that

$$\Gamma_P(pa, pa) = \frac{Z_\psi}{Z_P} - C_1 Z_\psi \frac{a^3 \langle \bar{q}q \rangle}{ma(pa)^2} + O(1/p^4). \quad (39)$$

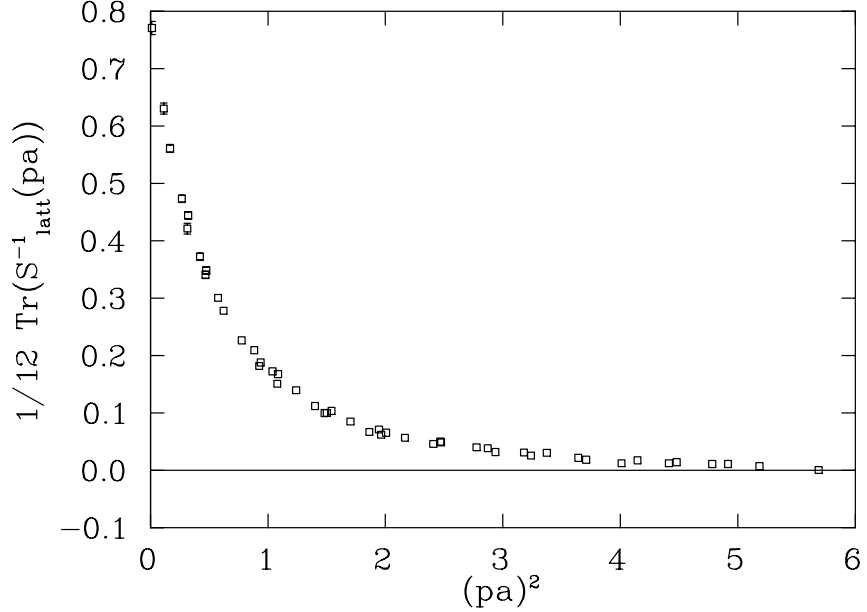


FIG. 4: The value of $\frac{1}{12}Tr(S_{latt}^{-1}(pa))$ extrapolated to $m = 0$ vs $(pa)^2$ by a simple linear extrapolation on $16^3 \times 28$ lattice. For large $(pa)^2$ the extrapolated value is zero within errors.

Since the quark condensate $\langle \bar{q}q \rangle$ has a contribution of $\frac{\langle |Q| \rangle}{mV}$ from the zero modes due to the topological charge Q , it is expected that $\Gamma_P(pa, pa)$ has $1/m^2$ and $1/m$ singularities as $m \rightarrow 0$. Thus, it is suggested [9] to fit $\Gamma_P(pa, pa)$ with the functional form involving pole terms. As illustrated in Fig. 6, the singular behavior in m is quite visible. It is suggested in Ref. [9] to fit the Γ_P with a double and single pole form for each pa

$$\Gamma_P(pa, pa) = \frac{c_{1,P}}{(am)^2} + \frac{c_{2,P}}{(am)} + c_{3,P} + c_{4,P}(am)^2. \quad (40)$$

This is appropriate for the case studied in Ref. [9] where the lattice volume is relatively small (the space-time volume is $\sim 10 \text{ fm}^4$) so that the zero mode contribution is substantial and the quark mass is relatively heavy so that the quenched chiral log is not significant. In our case, the space-time volume is 184 fm^4 , in which case the zero mode contribution is expected to be smaller. In our study of the quenched chiral log in the pion mass [29] with the same lattice, it is found that the pion mass is basically the same when calculated from either the $\langle PP \rangle$, $\langle A_4 P \rangle$, $\langle A_4 A_4 \rangle$, or $\langle PP - SS \rangle$ correlators, indicating that the zero mode effects are small and negligible within statistical errors, even for the smallest pion mass at $\sim 180 \text{ MeV}$. On the other hand, the quenched chiral log is quite prominent with pion mass less than 400 MeV . Therefore, we believe that the more appropriate approach is to relate

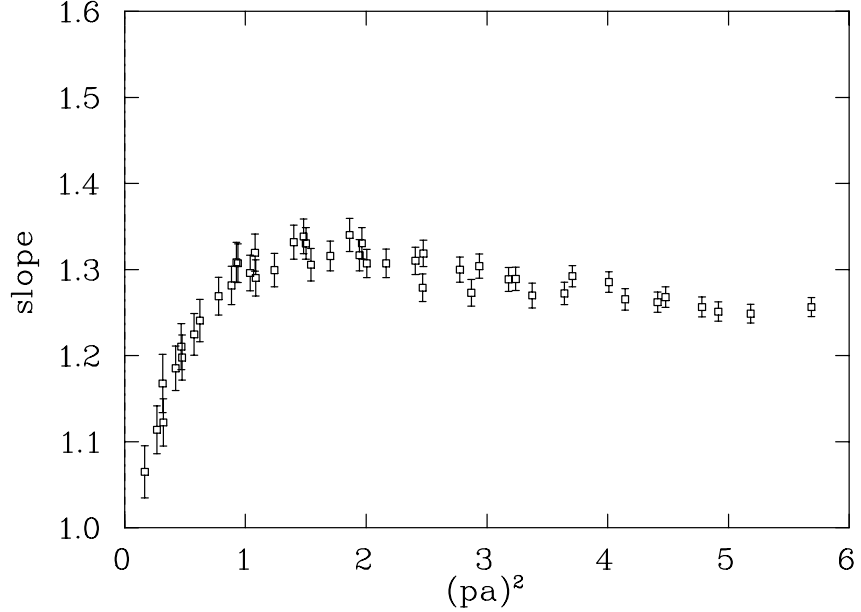


FIG. 5: A plot of the slope of $\frac{1}{12}Tr(S_{latt}^{-1}(pa))$ with respect to the quark mass. It is expected to be $Z_m Z_\psi$ at large $(pa)^2$ from Eq. (38)

the quark condensate in Eq. (39) to the pion mass through the Gell-Mann-Oakes-Renner relation

$$\langle \bar{\psi} \psi \rangle = -\frac{m_\pi^2 f_\pi^2}{2m}, \quad (41)$$

and use the power form for the pion mass where the leading log is re-summed through the cactus diagrams [38], i.e.

$$m_\pi^2(ma) = A(ma)^{\frac{1}{1+\delta}} + B(ma)^2. \quad (42)$$

Here δ is the quenched chiral log parameter.

Neglecting higher order terms and expanding $f_\pi \simeq f_\pi(0) + c(ma)$, we can approximate Eq. (39) as

$$\Gamma_{P,\text{latt}}(ap, ma) \simeq A_1 \left\{ (ma)^{\frac{1}{1+\delta}-2} + a_P(ma)^{\frac{1}{1+\delta}-1} \right\} + A_2 + C_P(ma^2) + D_P(ma)^2, \quad (43)$$

where

$$\begin{aligned} A_1 &= \frac{A a^3 f_\pi^2(0)}{2(pa)^2} C_1 Z_\psi, \\ a_P &= \frac{c}{f_\pi(0)}, \\ A_2 &= \frac{B a^3 f_\pi^2(0)}{2(pa)^2} C_1 Z_\psi + Z_m Z_\psi. \end{aligned} \quad (44)$$

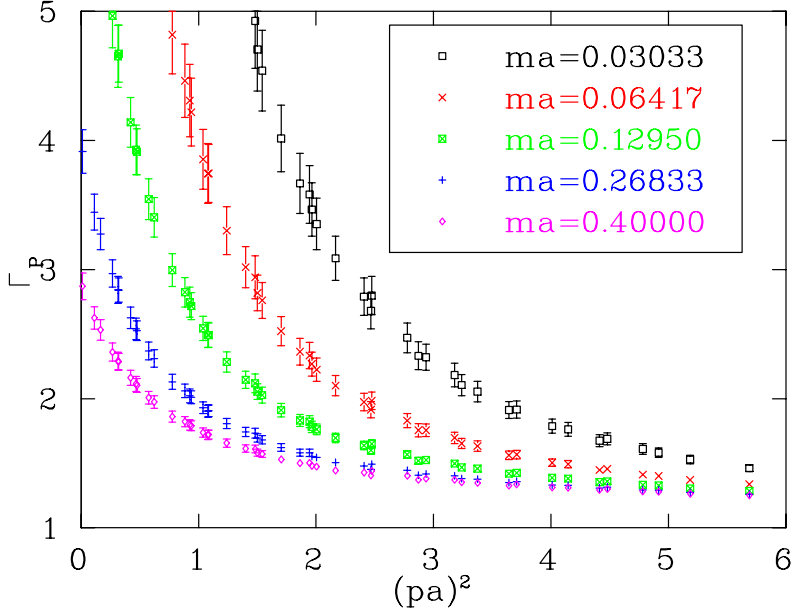


FIG. 6: Γ_P versus $(pa)^2$ with different masses. Here, one can clearly see the strong chiral log behavior.

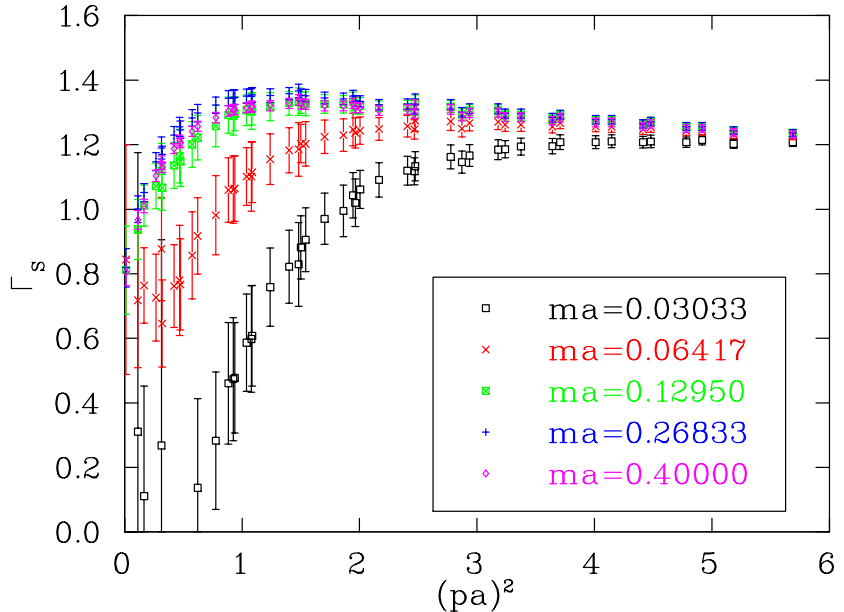


FIG. 7: Γ_S versus $(pa)^2$ with different masses. The chiral log behavior is also quite visible.

We plot $\Gamma_P(pa, pa)$ in Fig. 6 as a function of $(pa)^2$ for several ma . It is clear that at small $(pa)^2$, it has a singular behavior for small ma which is presumably due to the divergent terms associated with the quenched chiral δ .

From the vector Ward identity, one has the relation

$$\Gamma_S = \frac{1}{12} \frac{\partial \text{Tr}[S(p)^{-1}]}{\partial m} \quad (45)$$

From Eq. (38), the above Γ_S can be approximated with

$$\Gamma_S(pa, pa) = \frac{Z_\psi}{Z_S} + \frac{C_1 Z_\psi}{(pa)^2} \frac{\partial a^3 \langle \bar{q}q \rangle}{\partial ma} + \dots \quad (46)$$

for large $(pa)^2$.

Similar to the pseudo-scalar case, substituting the pion mass in Eq. (42) and the Gell-Mann-Oakes-Renner relation in Eq. (41) to Eq. (45) and neglecting the higher order terms beyond $(ma)^2$, we obtain

$$\begin{aligned} \Gamma_{S,\text{latt}}(ap, ma) = & A_1 \left\{ -\frac{\delta}{1+\delta} (ma)^{\frac{1}{1+\delta}-2} + a_S \frac{1}{1+\delta} (ma)^{\frac{1}{1+\delta}-1} \right\} \\ & + A_2 + C_S(ma^2) + D_S(ma)^2, \end{aligned} \quad (47)$$

At first glance, it appears that the quantity $Z_m Z_\psi$ is not separable in A_2 in Eq. (44). However, we should note that we know the values of A, B and $f_\pi(0)$ in Eq. (44) from an earlier study of pion mass and decay constant [29]. After fitting A_1 and A_2 in Eqs. (43) and (47), one can compare the first term in A_2 with A_1 to obtain $Z_m Z_\psi$. As we shall see later, it turns out the first term in A_2 is $O(10^{-2})$ times smaller than $Z_m Z_\psi$.

In order to obtain $Z_m Z_\psi$ and assess its finite ma error, we first subtract the divergent terms in Eqs. (43) and (47) and then fit the subtracted vertex functions linear and quadratic in m , i.e. with ma^2 and $m^2 a^2$ terms. In the following sub-section, we shall detail our fitting methods and give the results.

1. Fitting

We adopt the fitting procedure used to fit the chiral logs in pion mass [29] and the Roper resonance in the nucleon correlator [39] with priors. From the chiral log fit of the pion mass [29], we obtain δ to be in the range of $2.0 - - 1.5$ when the maximum pion mass for the fitting range is set to be ~ 500 MeV $- - 900$ MeV. Since we are fitting Γ_P and Γ_S in the similar quark mass range, we put a weak constraint on the value of δ with $\delta = 0.18(5)$ which covers the range of δ in the fit of the quenched chiral log in the pion mass. Data corresponding to the few lowest masses are first fitted with $A_{1P}(A_{1S}), a_P(a_S)$ and $A_{2P}(A_{2S})$

and then these parameters are constrained with those fitted values to fit the whole range of the masses with the forms in Eqs. (43) and (47). It is observed that these vertex functions are highly correlated between different masses and that the correlation increases with higher momentum. This, we believe, is due to the fact that the quark masses that we are interested in are all much smaller than the external momentum of $pa = 4.145$ which corresponds to $\mu = 2$ GeV that we will use to eventually match to the $\overline{\text{MS}}$ scheme at this scale. In this sense, the high correlation is a generic feature that this non-perturbative renormalization procedure faces for light quarks.

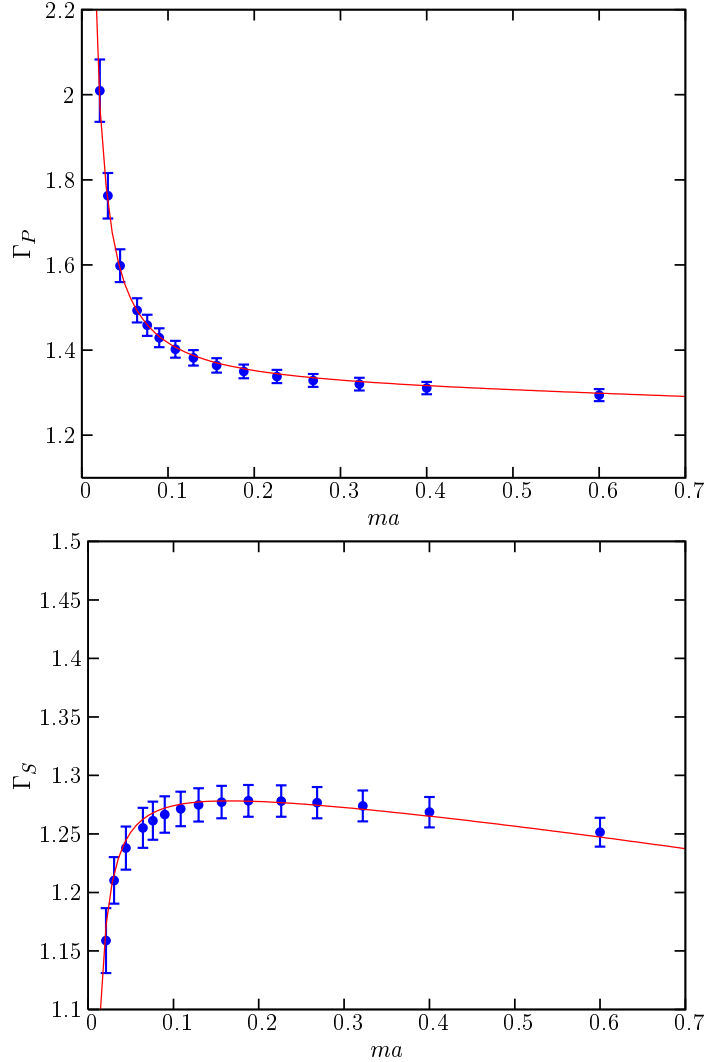


FIG. 8: Vertex functions for scalar (top) and pseudo-scalar (bottom) channels at the momentum corresponding to $\mu = 2$ GeV.

TABLE II: Fitted parameters corresponding to Eqs. (43) and (47)

Channel	A_1	$a_P(a_S)$	δ	A_2	C	D	χ^2/dof
P	0.008(1)	0.08(9)	0.163(18)	1.305(15)	-0.024(6)	-0.022(5)	1.29
S	0.011(5)	0.14(42)	0.171(24)	1.302(17)	-0.079(8)	-0.020(5)	1.47

We show in Fig. 8 the vertex functions $\Gamma_P(pa, ma)$ and $G_S(pa, ma)$ at $pa = 4.145$ as a function of ma , together with the fitted curves based on Eqs. (43) and (47). The fitted parameters are given in Table II. We see from the fitted parameters A_1, a, δ and A_2 from Γ_P agree with those fitted from Γ_S respectively, as we expected. This supports our supposition that the singular behaviors in both the $\Gamma_P(pa, ma)$ and $G_S(pa, ma)$ are due to the quenched chiral log in $\langle\bar{\psi}\psi\rangle$. We also tried to fit the pseudoscalar and scalar vertex functions Eq. (40) and found that the pole form does not fit well — the χ^2 is too large.

When we take the value of $A = 1.3$ and $B = 1.1$ from our pion mass chiral log fitting (Fig. 12 in Ref. [29]) in the relevant mass range, it follows from Eq. (44)

$$R = \frac{Ba^3 f_\pi^2(0)}{2(pa)^2} C_1 Z_\psi = \frac{BA_1}{A} = 0.0068, \quad (48)$$

which is two orders of magnitude smaller than A_2 . We shall subtract this contribution from A_2 to obtain $Z_m Z_\psi$ which changes its value by about half a σ which is not significant.

To eventually obtain Z_S and Z_P and their respective finite ma dependence, we define the subtracted Γ_P and Γ_S by taking out the divergent terms in Eqs. (43) and (47) and the first term in A_2 in Eq. (44) on each Jackknife sample (J) as

$$\Gamma_P^{sub,J}(ma) = \Gamma_P^J(ma) - A_{1J}^P \left\{ (ma)^{\frac{1}{1+\delta_J}-2} + a_J^P (ma)^{\frac{1}{1+\delta_J}-1} \right\} - \frac{BA_{1J}^P}{A}, \quad (49)$$

$$\Gamma_S^{sub,J}(ma) = \Gamma_S^J(ma) - A_{1J}^S \left\{ -\frac{\delta_J}{1+\delta_J} (ma)^{\frac{1}{1+\delta_J}-2} + \frac{a_J^S}{1+\delta_J} (ma)^{\frac{1}{1+\delta_J}-1} \right\} - \frac{BA_{1J}^S}{A}. \quad (50)$$

From Eqs. (43), (44), (47), and (49), we see that the ratios of Z_ψ/Z_P and Z_ψ/Z_S are the subtracted vertices Γ_P and Γ_S at the massless limit for each pa in the RI scheme, i.e.

$$\frac{Z_\psi(pa)}{Z_{P,S}(pa)} = \Gamma_{P,S}^{sub}(pa, ma = 0). \quad (51)$$

We plot in Fig. 9, Z_ψ/Z_P , Z_ψ/Z_S , and the ratio Z_S/Z_P as a function of $(pa)^2$. We see that for $(pa)^2 > 3$, the ratio goes to unity which is a confirmation that our fitting procedure does not spoil the expected chiral property $Z_P = Z_S$ for the overlap fermion.

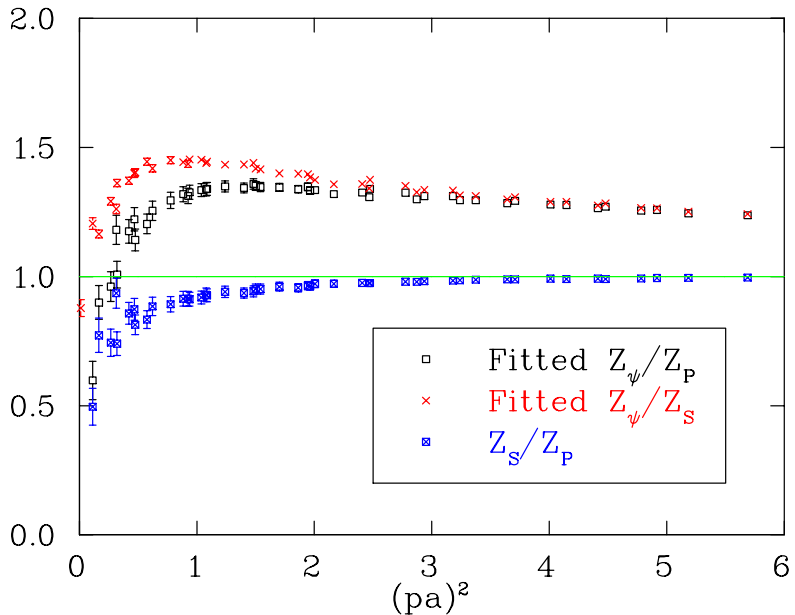


FIG. 9: Z_ψ/Z_P and Z_ψ/Z_S and the ratio Z_P/Z_S as a function of $(pa)^2$.

C. The tensor current

In Fig. 10, we show Γ_T versus $(pa)^2$ with different masses. We can see that at moderate to large $(pa)^2$, Γ_T is not sensitive to the quark masses. The chiral limit value is obtained by a linear plus quadratic fitting as for the case of vector and axial vector currents and the results will be presented in the next section.

V. RUNNING OF THE RENORMALIZATION CONSTANTS

In general, one can choose to define the renormalization conditions for different p and p' in Eq. (10). But the virtualities of the quark states must be much larger than Λ_{QCD} . This is so because in order to obtain physical results at certain scale (e.g. momentum or mass), one needs to combine the matrix element of the renormalized operator $O(\mu)$ with the Wilson coefficient function. The latter is usually computed in continuum perturbation theory by expanding in $\alpha_s^{\overline{\text{MS}}}$ at a scale of order of μ . Thus, for the validity of perturbation calculation, μ must be large. On the other hand, one would like to have $\mu \ll 1/a$ in order to have smaller $O(a)$ effects. When spontaneous symmetry breaking takes place, as is in QCD, a large μ may not be enough due to the presence of the Goldstone boson. For example, at low momentum transfer $q = p' - p$, the Green's function can have a Goldstone boson

pole like $1/q^2$. However for fermions (but not for a scalar particle), this contribution will be $1/p^2 = 1/\mu^2$ smaller than the perturbative contribution even when $q^2 = 0$ [1]. Thus, it is desirable to have a window $\Lambda_{QCD} \ll \mu \ll 1/a$ so that both the non-perturbative effects and the lattice artifacts are small. In practice, one finds that the renormalization procedure prescribed here works well for $(\mu a)^2$ as large as 6. In the current case, this corresponds to $\mu \sim 2.5$ GeV.

The renormalized operators are defined as

$$Z_O O_{\text{bare}} = O_{\text{ren}}. \quad (52)$$

The fact that the bare operator is independent of the renormalization scale μ^2 gives the renormalization group (RG) equation,

$$\mu^2 \frac{d}{d\mu^2} O_{\text{ren}} = \frac{1}{Z_O} \mu^2 \frac{dZ_O}{d\mu^2} O_{\text{ren}} \quad (53)$$

$$= -\frac{\gamma_O}{2} O_{\text{ren}}. \quad (54)$$

where

$$\gamma_O = -\frac{2\mu^2}{Z_O} \frac{dZ_O}{d\mu^2}, \quad (55)$$

is the anomalous dimension.

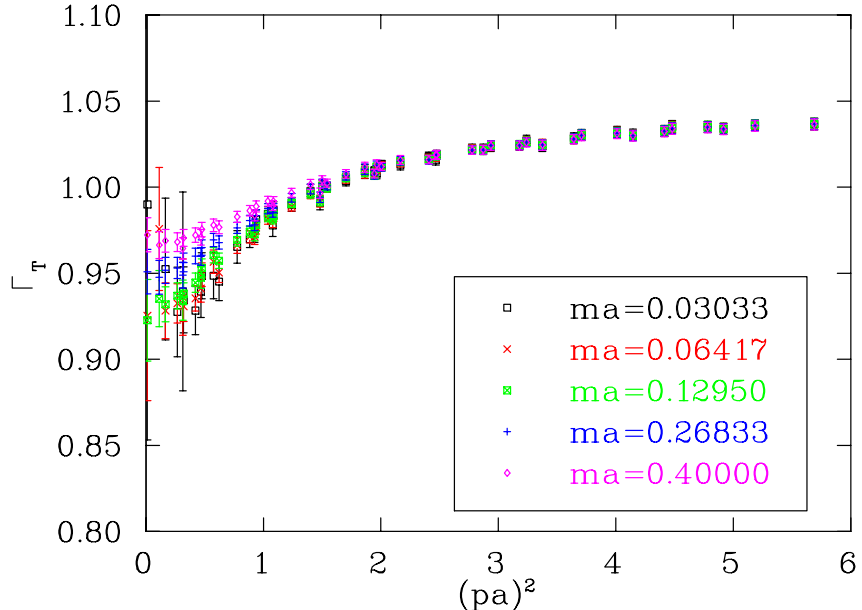


FIG. 10: Γ_T versus $(pa)^2$ with different masses. It has no significant mass dependence

The solution of $Z_O(\mu^2)$ can be written in the following form

$$Z_O(\mu^2) = \frac{C_O(\mu^2)}{C_O(\mu'^2)} Z_O(\mu'^2). \quad (56)$$

Expanding the anomalous dimension in the coupling constant α_s

$$\gamma_O = \sum_i \gamma_O^{(i)} \left(\frac{\alpha_s}{4\pi} \right)^{i+1}, \quad (57)$$

and considering the running of α_s in QCD β function $\beta(\alpha_s)$ perturbatively

$$\frac{\beta(\alpha_s)}{4\pi} = \mu^2 \frac{d}{d\mu^2} \left(\frac{\alpha_s}{4\pi} \right) = - \sum_{i=0}^{\infty} \beta_i \left(\frac{\alpha_s}{4\pi} \right)^{i+2}, \quad (58)$$

where β_i are the coefficients of the QCD β function $\beta(\alpha_s)$, one can solve for the coefficient functions C_O perturbatively.

The four loop solution [40] of the coefficient function in Eq. (56) is (we have suppressed the subscripts for the specific operator O)

$$\begin{aligned} C(\mu^2) = & \left(\frac{\alpha_s(\mu)}{\pi} \right)^{\bar{\gamma}_0} \left\{ 1 + \left(\frac{\alpha_s(\mu)}{4\pi} \right) (\bar{\gamma}_1 - \bar{\beta}_1 \bar{\gamma}_0) \right. \\ & + \frac{1}{2} \left(\frac{\alpha_s(\mu)}{4\pi} \right)^2 \left[(\bar{\gamma}_1 - \bar{\beta}_1 \bar{\gamma}_0)^2 + \bar{\gamma}_2 + \bar{\beta}_1^2 \bar{\gamma}_0 - \bar{\beta}_1 \bar{\gamma}_1 - \bar{\beta}_2 \bar{\gamma}_0 \right] \\ & + \left(\frac{\alpha_s(\mu)}{4\pi} \right)^3 \left[\frac{1}{6} (\bar{\gamma}_1 - \bar{\beta}_1 \bar{\gamma}_0)^3 + \frac{1}{2} (\bar{\gamma}_1 - \bar{\beta}_1 \bar{\gamma}_0) (\bar{\gamma}_2 + \bar{\beta}_1^2 \bar{\gamma}_0 - \bar{\beta}_1 \bar{\gamma}_1 - \bar{\beta}_2 \bar{\gamma}_0) \right. \\ & \left. \left. + \frac{1}{3} \left(\bar{\gamma}_3 - \bar{\beta}_1^3 \bar{\gamma}_0 + 2\bar{\beta}_1 \bar{\beta}_2 \bar{\gamma}_0 - \bar{\beta}_3 \bar{\gamma}_0 + \bar{\beta}_1^2 \bar{\gamma}_1 - \bar{\beta}_2 \bar{\gamma}_1 - \bar{\beta}_1 \bar{\gamma}_2 \right) \right] \right\}, \end{aligned} \quad (59)$$

where

$$\bar{\gamma}_{Oi} = \frac{\gamma_O^{(i)}}{2\beta_0}, \quad \bar{\beta}_i = \frac{\beta_i}{\beta_0}. \quad (60)$$

The following tables give the anomalous dimensions $\gamma^{(i)}$ for Z_ψ , Z_m and Z_T in the RI/MOM scheme for the quenched approximation [19, 40, 41]. In the case of chiral fermions, $Z_S = Z_P = 1/Z_m$, so that $C_S(\mu^2) = C_P(\mu^2) = 1/C_m(\mu^2)$. Note that, in Refs. [19, 40, 41], the definition of Z 's is the inverse of our definition in (Eq. (52)).

The coupling constant itself is running with respect to μ . The four loop formula is given

TABLE III: Quenched Z_ψ Anomalous Dimensions $\gamma_\psi^{(i)}$

$\gamma^{(0)}$	$\gamma^{(1)}$	$\gamma^{(2)}$	$\gamma^{(3)}$
0	44.6667	2177.0737	130760.2969

 TABLE IV: Quenched Z_m Anomalous Dimensions $\gamma_m^{(i)}$

$\gamma^{(0)}$	$\gamma^{(1)}$	$\gamma^{(2)}$	$\gamma^{(3)}$
8	252	11769.5469	557837.9375

 TABLE V: Quenched Z_T Anomalous Dimensions $\gamma_T^{(i)}$

$\gamma^{(0)}$	$\gamma^{(1)}$	$\gamma^{(2)}$
2.66667	80.4444	3268.2996

by [42]

$$\begin{aligned}
 \frac{\alpha_s}{4\pi} = & \frac{1}{\beta_0 \ln(\mu^2/\Lambda_{QCD}^2)} - \frac{\beta_1 \ln \ln(\mu^2/\Lambda_{QCD}^2)}{\beta_0^3 \ln^2(\mu^2/\Lambda_{QCD}^2)} \\
 & + \frac{1}{\beta_0^5 \ln^3(\mu^2/\Lambda_{QCD}^2)} \left\{ \beta_1^2 \ln^2 \ln(\mu^2/\Lambda_{QCD}^2) - \beta_1^2 \ln \ln(\mu^2/\Lambda_{QCD}^2) \right. \\
 & \left. + \beta_2 \beta_0 - \beta_1^2 \right\} + \frac{1}{\beta_0^7 \ln^4(\mu^2/\Lambda_{QCD}^2)} \left\{ \beta_1^3 \ln^3 \ln(\mu^2/\Lambda_{QCD}^2) \right. \\
 & - \frac{5}{2} \beta_1^3 \ln^2 \ln(\mu^2/\Lambda_{QCD}^2) - (2\beta_1^3 - 3\beta_0 \beta_1 \beta_2) \ln \ln(\mu^2/\Lambda_{QCD}^2) \\
 & \left. + \frac{1}{2} (\beta_1^3 - 3\beta_0^2 \beta_3) \right\}
 \end{aligned} \tag{61}$$

The QCD β -function is scheme independent only up to two loops. The additional term of the expansion has been computed in the $\overline{\text{MS}}$ scheme in [43].

In this work, the value of α_s was calculated at four loops using a lattice value of Λ_{QCD} taken from Ref. [44] as

$$\Lambda_{\text{QCD}} = 238 \pm 19 \text{ MeV}. \tag{62}$$

Both Z_A and Z_V are scale independent, but this is not the case for Z_ψ . The scale invariant

(SI) vertex for the axial and vector current is defined by removing the renormalization group running of Z_ψ as

$$\Gamma_{A,V}^{\text{SI}}((ap)^2) = \Gamma_{A,V}((ap)^2) / C_\psi((ap)^2), \quad (63)$$

where C_ψ is defined in Eq. (59) with the anomalous dimension coefficients from Table III. We normalize $C_\psi((\mu a)^2 = 4.10) = 1$, which corresponds to $\mu = 2.0$ GeV, in order to compare with the $(pa)^2$ dependence of $\Gamma_{A,V}((ap)^2)$.

Fig. 11 shows both $\Gamma_A((ap)^2, ma = 0)$ and $\Gamma_A^{\text{SI}}((ap)^2, ma = 0)$ as a function of $(pa)^2$. By comparing them, we see that the renormalization group running due to Z_ψ is not appreciable for $(pa)^2 > 3$, but it does tend to make the SI data flatter as a function of $(pa)^2$. The remaining scale dependence of $\Gamma_A^{\text{SI}}((ap)^2, ma = 0)$ is very small. A plausible explanation for it is an $(ap)^2$ error [9]. Fitting the remaining scale dependence to the form [9]

$$\Gamma_A^{\text{SI}}((ap)^2) = \Gamma_A^{\text{SI}} + c(ap)^2, \quad (64)$$

for a range of momenta that is chosen to be “above” the region where the condensate effects are important, one can obtain the scale invariant Γ_A which is denoted as Γ_A^{SI} .

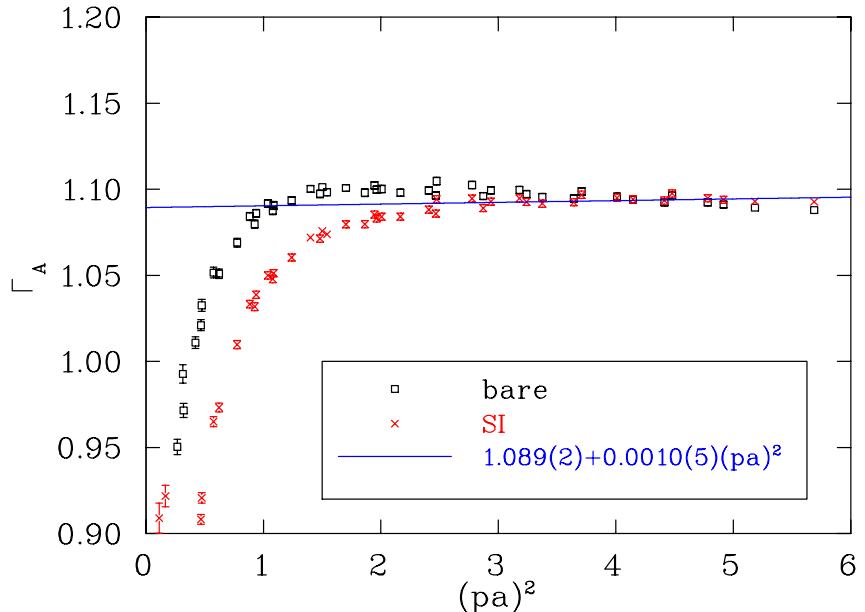


FIG. 11: Γ_A (labeled as “bare”) and the scale invariant Γ_A^{SI} versus $(pa)^2$ in the chiral limit. They coincide at $(pa)^2 = 4$. The later is almost $(pa)^2$ independent after $(pa)^2 > 2.4$, the slope versus $(pa)^2$ is about 0.001. For ideal case, the slope should be zero, and this small value can be interpreted as an $O(a^2)$ error.

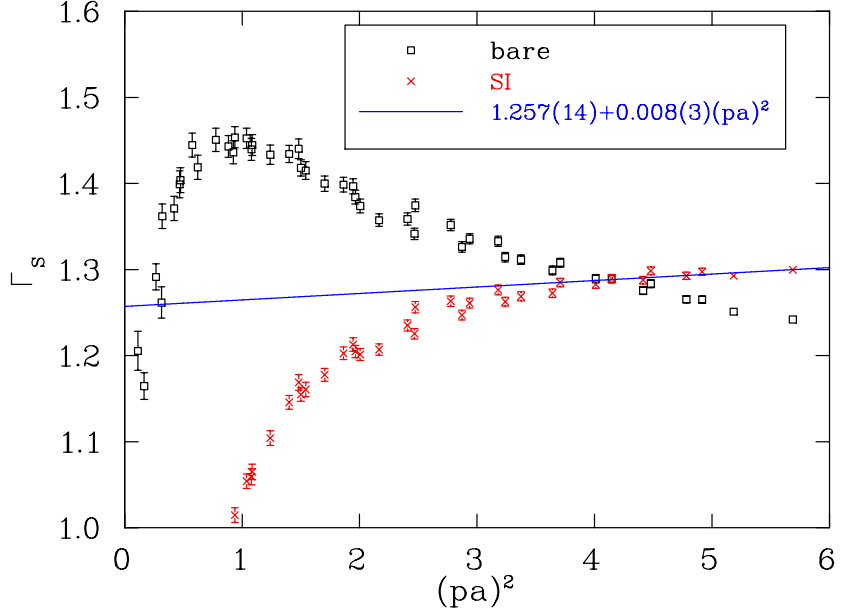


FIG. 12: The same as Fig. (11) for Γ_S and Γ_S^{SI} . The slope of SI versus $(pa)^2$ is about 0.008 beyond $(pa)^2 \geq 4.0$, this small value can be interpreted as an $O(a^2)$ error.

When a linear fit of the SI data versus $(ap)^2$ is performed, for $2.4 < (ap)^2 < 5.7$, the gradient is ≈ 0.001 . In the ideal case, the gradient should be zero, this small value is interpreted as an $O(a^2)$ error. This shows the ratio of the Z_ψ and Z_A $(pa)^2$ errors is small, but we don't know their individual $(pa)^2$ error separately. It appears that the $(pa)^2$ error in Z'_ψ as defined from the quark propagator in Eq. (19) is as large as $\sim 10\%$ at $p = 2$ GeV [9, 45]. However, this relatively large $(pa)^2$ error in Z_ψ^{SI} must be canceled to a large extent by that of Z_A , resulting in a small $(pa)^2$ error in Γ_A^{SI} (only 0.4% at $(pa)^2 = 4.1$). As will be discussed in the next sub-section, we will use Z_A determined from the chiral Ward identity to obtain Z_ψ . Since Z_A , in this case, is determined from the pion state at rest, it is at a momentum scale of Λ_{QCD} . Thus, it should have small $(pa)^2$ error. Using this value of Z_A and $\Gamma_A^{\text{SI}}((ap)^2, ma = 0)$ to obtain Z_ψ^{SI} , and thus $Z_\psi^{RI}(2 \text{ GeV})$ should give a $(pa)^2$ error of $\sim 0.4\%$ which we shall consider as the systematic error in $O(a^2)$.

In the case of $\Gamma_S^{\text{sub}} = Z_\psi/Z_S$, both Z_ψ and Z_S run with $(\mu)^2$. Fig. 12 shows Γ_S^{sub} and the corresponding scale invariant (SI) vertex – $\Gamma_S^{\text{sub,SI}}$, after three loop running. We see that $\Gamma_S^{\text{sub,SI}}$ is much flatter than Γ_S^{sub} for $(pa)^2 > 3.0$. The linear fit of the SI data versus $(ap)^2$ in the range of $4.0 < (ap)^2 < 5.7$, gives a gradient of 0.008(3). This is an order of magnitude larger than that of the axial vector (and that of the tensor current below). This

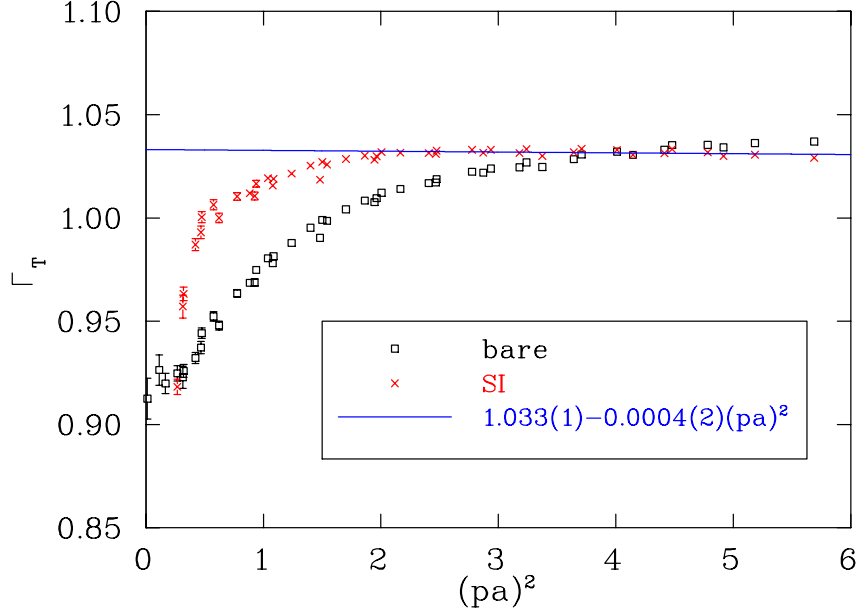


FIG. 13: The same as Fig. (11) for Γ_T and Γ_T^{SI} . The later is almost $(pa)^2$ independent after $(pa)^2 > 2.0$, the slope versus $(pa)^2$ is about -0.0004 , this small value can be interpreted as an $O(a^2)$ error.

relatively larger gradient could be due to the systematic uncertainty in subtracting the chiral divergence in Γ_S or the mismatch of the $(pa)^2$ errors between Z_{ψ}^{SI} and Z_S^{SI} or both.

The SI result of Γ_T which comes from the three loop running of Z_T [41] and four loop running of Z_{ψ} is plotted in Fig. 13 along with Γ_T . The linear fit to the SI data in the range of $2.0 < (ap)^2 < 5.7$ gives a gradient of $-0.0004(2)$.

It is worthwhile pointing out that comparing to the Domain Wall fermion case on a $16^3 \times 32 \times 16$ lattice with Wilson gauge action at $\beta = 6.0$ [9], we find that the remaining scale dependence as measured by the gradient in $(pa)^2$ are comparable for the Γ_S^{SI} . But the gradient for $\Gamma_A^{\text{SI}}/\Gamma_T^{\text{SI}}$ is one/two orders of magnitude smaller than that in the Domain Wall fermion case. Since the Domain Wall fermion with finite 5th dimension and the rational polynomial approximation of the sign function that we adopt in the present work are two different approximations of the same overlap fermion in 4 dimensions [46], the $(pa)^2$ errors in the scale invariant vertices serve as a measure of the $O(a^2)$ error of the approximation.

A. Determining Z_A from Ward identity

Before applying the renormalization group running (an inverse operation of Eq. (63)) to match to the $\overline{\text{MS}}$ scheme at certain scale, we need to input Z_A to Γ_A to obtain Z_ψ , which, then in turn, can determine other renormalization constants from the respective vertex functions. As explained in Sec. II B), we prefer using Z_A from the chiral Ward identity to determine Z_ψ than directly obtaining it from the quark propagator. This is partly due to the fact that there is ambiguity in the lattice definition of momentum [9] in Eq. 19. Furthermore, it is shown in the study with Domain Wall fermion [9] and an earlier study of the overlap fermion [45] that the $(pa)^2$ errors in the scale invariant Z_ψ^{SI} are quite large. As a result, these factors can introduce 10% -- 20% uncertainty [9].

The renormalization constant Z_A for the axial current $A_\mu = \bar{\psi}(i\gamma_\mu\gamma_5(1 - D/2\rho)\frac{\tau^a}{2})\psi$ can be obtained directly through the axial Ward identity

$$Z_A \partial_\mu A_\mu = 2Z_m m Z_P P, \quad (65)$$

where $P = \bar{\psi}(i\gamma_5(1 - D/2\rho)\frac{\tau^a}{2})\psi$ is the pseudo-scalar density. For the case of the overlap fermion [18, 20], $Z_m = Z_S^{-1}$ and $Z_S = Z_P$. Thus, Z_m and Z_P cancel in Eq. (65) and one can determine Z_A to $O(a^2)$ non-perturbatively from the axial Ward identity using the bare mass m and bare operator P . To obtain Z_A , we shall consider the on-shell matrix elements between the vacuum and the zero-momentum pion state for the axial Ward identity

$$Z_A \langle 0 | \partial_\mu A_\mu | \pi(\vec{p} = 0) \rangle = 2m \langle 0 | P | \pi(\vec{p} = 0) \rangle, \quad (66)$$

where the matrix elements can be obtained from the zero-momentum correlators

$$\begin{aligned} G_{\partial_4 A_4 P}(\vec{p} = 0, t) &= \langle \sum_{\vec{x}} \partial_4 A_4(x) P(0) \rangle \\ G_{PP}(\vec{p} = 0, t) &= \langle \sum_{\vec{x}} P(x) P(0) \rangle. \end{aligned} \quad (67)$$

The non-perturbative Z_A is then

$$Z_A = \lim_{m \rightarrow 0, t \rightarrow \infty} \frac{2m G_{PP}(\vec{p} = 0, t)}{G_{\partial_4 A_4 P}(\vec{p} = 0, t)}. \quad (68)$$

Given that the time derivative itself in $G_{\partial_4 A_4 P}(\vec{p} = 0, t)$ invokes an $O(a^2)$ error, it would be better to adopt a definition for Z_A which is devoid of this superfluous $O(a^2)$ error. This

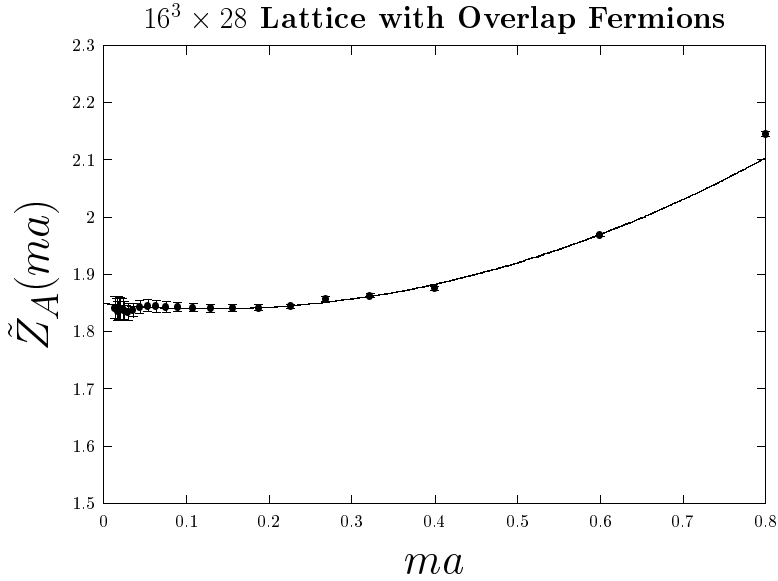


FIG. 14: $\tilde{Z}_A(ma)$ vs quark mass ma .

can be achieved by noticing that, at large t where the pion state dominates the propagator $G_{\partial_4 A_4 P}(\vec{p} = 0, t)$, one can effectively make the substitution

$$G_{\partial_4 A_4 P}(\vec{p} = 0, t) \xrightarrow[t \rightarrow \infty]{} m_\pi G_{A_4 P}(\vec{p} = 0, t). \quad (69)$$

Consequently, Eq. (68) becomes

$$Z_A = \lim_{m \rightarrow 0, t \rightarrow \infty} \frac{2m G_{PP}(\vec{p} = 0, t)}{m_\pi G_{A_4 P}(\vec{p} = 0, t)}. \quad (70)$$

Since the G_{PP} and $G_{A_4 P}$ correlators are calculated at finite ma , we shall define the renormalization factor

$$\tilde{Z}_A(ma) = \lim_{t \rightarrow \infty} \frac{2m G_{PP}(\vec{p} = 0, t)}{m_\pi G_{A_4 P}(\vec{p} = 0, t)}, \quad (71)$$

where the massless limit would give Z_A . In view of the fact that there is no $O(a)$ error with the overlap fermion, $\tilde{Z}_A(ma)$ should have the form [16, 20]

$$\tilde{Z}_A(ma) = Z_A(1 + b_A m \Lambda_{QCD} a^2 + c_A m^2 a^2) \quad (72)$$

at $O(a^2)$ and $\Lambda_{QCD} = 0.238$ GeV. We plot the results of $\tilde{Z}_A(ma)$ from Eq. (71) in Fig. (14). As noticed before [20], it is conspicuously flat as a function of ma indicating that the $O(a^2)$ error from the action and the axial-vector operator is small. From the fitting to the form in Eq. (72) for the range of ma from 0.014 to 0.6, we find that $Z_A = 1.849(4)$, $b_A = -0.347(16)$, $c_A = 0.317(21)$ with $\chi^2/dof = 0.54$.

We observe that Z_A is determined to the precision of 0.2% in statistical error. It is thus more desirable [9] to use Z_A from the Ward identity to determine Z_ψ from Γ_A and use it to find all the other renormalization constants.

From the renormalization condition Eq. (22), we finally obtain the SI Z_ψ^{SI}

$$Z_\psi^{\text{SI}} = Z_A \Gamma_A^{\text{SI}}, \quad (73)$$

which in term can be used to determine the other SI renormalization constants

$$Z_O^{\text{SI}} = \frac{Z_\psi^{\text{SI}}}{\Gamma_O^{\text{SI}}}. \quad (74)$$

Since we normalize the scale invariant vertex functions to those RI scheme at $(pa)^2 = 4.1$, the renormalization constant determined in Eq. (74) is just $Z_O^{RI}(\mu = 2 \text{ GeV})$.

B. Matching to $\overline{\text{MS}}$ scheme

In order to confront experiments, one frequently likes to quote the final results in the $\overline{\text{MS}}$ scheme at certain scale. For light hadrons, the popular scale is 2 GeV. To obtain the renormalization constants in the $\overline{\text{MS}}$ scheme at 2 GeV, one can use the perturbatively computed coefficient functions in Eq. (59) in the $\overline{\text{MS}}$ scheme to evolve the scale invariant renormalization constant to the targeted scale, i.e.

$$Z_O^{\overline{\text{MS}}}(\mu) = C_O^{\overline{\text{MS}}}(\mu) Z_O^{\text{SI}}. \quad (75)$$

Alternatively, one can avoid the step of going to the scale invariant quantity and, instead, match directly from the RI-scheme to the $\overline{\text{MS}}$ scheme at the same scale. The perturbative expansion of the ratio $Z^{\overline{\text{MS}}}/Z^{RI}$ to two-loop order are given by the finite coefficients in the perturbative expansion of Z^{RI} [19]

$$R = \frac{Z^{\overline{\text{MS}}}}{Z^{RI}} = 1 + \frac{\alpha_s}{4\pi} (Z^{RI})_0^{(1)} + \left(\frac{\alpha_s}{4\pi}\right)^2 (Z^{RI})_0^{(2)} + \dots \quad (76)$$

The numerical values of the matching coefficients, $Z_0^{(1)}$, $Z_0^{(2)}$ and $Z_0^{(3)}$ in Eq. (76) used for Z_ψ , Z_m and Z_T have been calculated in Ref. [40] and Ref. [47], and are collected in Table VI.

The final results for the renormalization constants are listed in Table VII. The results for Z_A , Z_V , Z_P , Z_S , Z_T and Z_ψ in the RI and $\overline{\text{MS}}$ scheme at 2 GeV (for Z_P , Z_S , Z_T and Z_ψ) are listed in Table VII.

TABLE VI: Quenched RI to $\overline{\text{MS}}$ matching coefficients

$Z_{(0)}$	$Z_0^{(1)}$	$Z_0^{(2)}$	$Z_0^{(3)}$	R at 2 GeV
Z_ψ	0.0000	-25.4642	-1489.9805	0.98706
Z_m	-5.3333	-149.0402	-5598.9526	0.85127
Z_T	0.0000	-46.6654	-2067.9753	0.97909

 TABLE VII: Renormalization constants Z in RI, and $\overline{\text{MS}}$ schemes at $\mu = 2$ GeV. The renormalization constant in the SI scheme is normalized to be the same as that in the RI scheme at 2 GeV. These Z – factors are obtained from the lattice with $a = 0.200$ fm.

Z – factor	RI at 2 GeV	$\overline{\text{MS}}$ at 2 GeV
Z_A	1.853(9)	1.853(9)
Z_V	1.846(8)	1.846(8)
Z_P	1.571(15)	1.845(17)
Z_S	1.567(13)	1.841(15)
Z_T	1.966(6)	1.925(6)
Z_ψ	2.307(18)	2.277(18)

VI. FINITE ma CORRECTION OF THE RENORMALIZATION CONSTANT

Similar to the renormalization factor $\tilde{Z}_A(ma)$ defined in Eqs. (71) and (72) for the axial current, we shall define the renormalization factor for the other operators by

$$\tilde{Z}_O(ma) = Z_O(\mu a, g(a))(1 + b_O m(\Lambda_{QCD})a^2 + c_O(ma)^2) \quad (77)$$

to reflect the finite ma corrections of the renormalization constants, where $O = V, S, P, T$ and ψ . To obtain the renormalization factors for $O = V, S, P, T$ and ψ , we shall adopt the same renormalization condition Eq. (14) for finite ma . This is consistent with the mass-independent renormalization scheme. We shall use the quark propagator to obtain the finite ma dependence for $\tilde{Z}_\psi(ma)$ from Eq. (19), except with $Z_\psi = \tilde{Z}_\psi(ma = 0)$ normalized from Z_A via the renormalization condition, Eq. (22). We then follow the above procedure in the preceding sections to obtain $\tilde{Z}_A(ma), \tilde{Z}_V(ma), \tilde{Z}_S(ma), \tilde{Z}_P(ma)$, and $\tilde{Z}_T(ma)$. The $\tilde{Z}_\psi^{\overline{\text{MS}}}(ma, \mu = 2 \text{ GeV})$ for $\tilde{Z}_\psi(ma)$ in the $\overline{\text{MS}}$ scheme at $\mu = 2$ GeV is plotted in Fig. 20. The

corresponding results on $\tilde{Z}_A(ma)$, $\tilde{Z}_V(ma)$, $\tilde{Z}_S^{\overline{\text{MS}}}(ma, \mu = 2 \text{ GeV})$, $\tilde{Z}_P^{\overline{\text{MS}}}(ma, \mu = 2 \text{ GeV})$ and $\tilde{Z}_T^{\overline{\text{MS}}}(ma, \mu = 2 \text{ GeV})$ are plotted in Fig. 15, 16, 18, 17 and 19 respectively.

We observe that these curves are all rather flat, with less than 3% correction for ma as large as 0.6. We make a correlated fit of the finite ma behavior with the form in Eq. (77). The coefficients b_O and c_O are listed in Table VIII. The fitted curves are drawn in Figs. 15, 16, 18, 17 and 19 as solid lines. For comparison, we also plot the uncorrelated fits as dashed lines which have much smaller χ^2/dof than those of the correlated fits. The flatness in ma reflects the fact that the $O((ma)^2)$ corrections are small. This is consistent with the findings in the π and ρ masses [18] and their dispersion relations [16]. The observed small $O(ma^2)$ and $O(m^2a^2)$ errors are much smaller than those found with the chirally improved Dirac operator [10]. We don't know the finite ma behavior of the domain-wall fermion from the study of the quark bilinear operators [9]. The study of $\tilde{Z}_A(ma)$ and $\tilde{Z}_V(ma)$ from the nucleon matrix elements found much larger $O(ma^2)$ and $O(m^2a^2)$ errors than observed here.

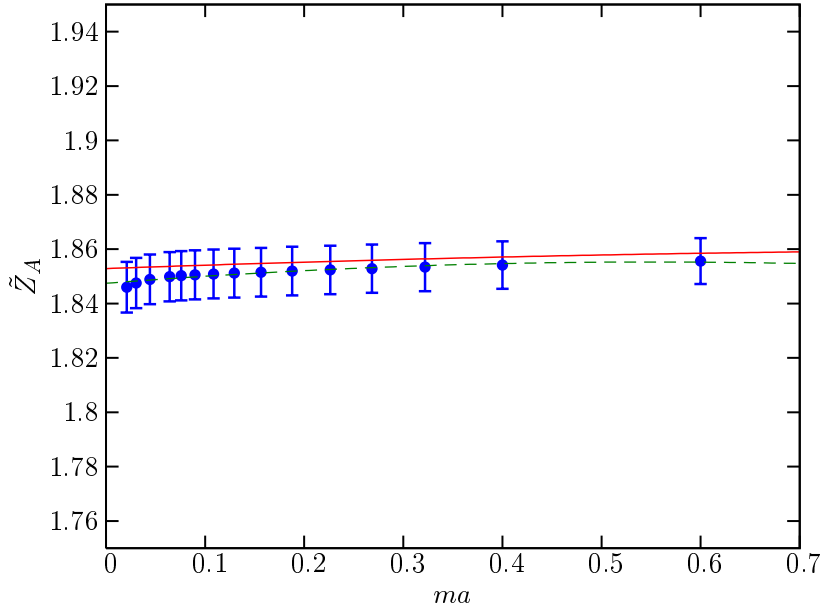
We should point out that in Sec. V A, $\tilde{Z}_A(ma)$ was defined in Eqs. (71) and (72) with the implicit assumption that $\tilde{Z}_P(ma)$ is not very different from $\tilde{Z}_S(ma)$ for the available range of ma . Even though this does not in principle affect the extraction of the renormalization constant Z_A at the massless limit of $\tilde{Z}_A(ma)$, where Z_P is equal to Z_S , the extrapolation could have a large uncertainty if $\tilde{Z}_P(ma)$ is very different from $\tilde{Z}_S(ma)$ for the range of ma which is not close to the chiral limit. Thus, it is gratifying to see in Figs. 17 and 18 that the ma behaviors of $\tilde{Z}_P(ma)$ and $\tilde{Z}_S(ma)$ (in the $\overline{\text{MS}}$ scheme at 2 GeV in this case) are very similar. They differ less than 3% for $ma \leq 0.6$. The upshot is that we should take the ma behavior in $\tilde{Z}_A(ma)$ in Fig. 15 as the correct one, instead of that in Fig. 14 as defined in Eq. (71). Any attempt to correct for the negligence of the ma dependence in $\tilde{Z}_P(ma)$ and $\tilde{Z}_S(ma)$ in Eq. (71) and compare with that in $\tilde{Z}_A(ma)$ in Fig. 15 is expected to reflect different finite ma corrections under different renormalization conditions.

VII. SUMMARY AND OUTLOOK

In this work, we performed a non-perturbative renormalization calculation of the composite quark bilinear operators with the overlap fermion in the regularization-independent scheme from the quark vertex function with high virtuality. The renormalization group running of the renormalization constants were calculated to obtain the scale invariant (SI)

TABLE VIII: Mass dependence of the renormalization factors

	$Z_O^{\overline{\text{MS}}}$ (2 GeV)	b_O	c_O	χ^2/dof
A	1.853(9)	0.029(16)	-0.003(2)	1.3
V	1.846(8)	-0.0055(33)	-0.013(7)	2.20
P	1.845(20)	-0.015(12)	0.017(4)	0.3
S	1.841(15)	0.22(19)	0.004(2)	0.7
T	1.925(6)	-0.012(8)	-0.015(3)	1.6
ψ	2.277(18)	-0.001(2)	0.002(1)	0.8


 FIG. 15: Renormalization factor $\tilde{Z}_A(ma)$ against quark mass ma . The solid line is the correlated fit and the dashed line is the uncorrelated fit.

renormalization constants and also matched to the $\overline{\text{MS}}$ scheme at $\mu = 2$ GeV. The scale invariant Z_A , obtained from the Ward identity, was used to obtain the wavefunction renormalization Z_ψ which, in turn, determined the other constants. Since Z_A , as determined from the Ward identity, has very small error ($\sim 0.2\%$), it is more desirable to use it to determine Z_ψ instead of using the quark propagator to determine Z_ψ which can introduce an error as large as $\sim 10\%$.

After subtracting the quenched chiral log divergences in the vertex functions Γ_P and Γ_P due to the presence of the pseudoscalar meson, the expected relations $Z_S = Z_P$ and

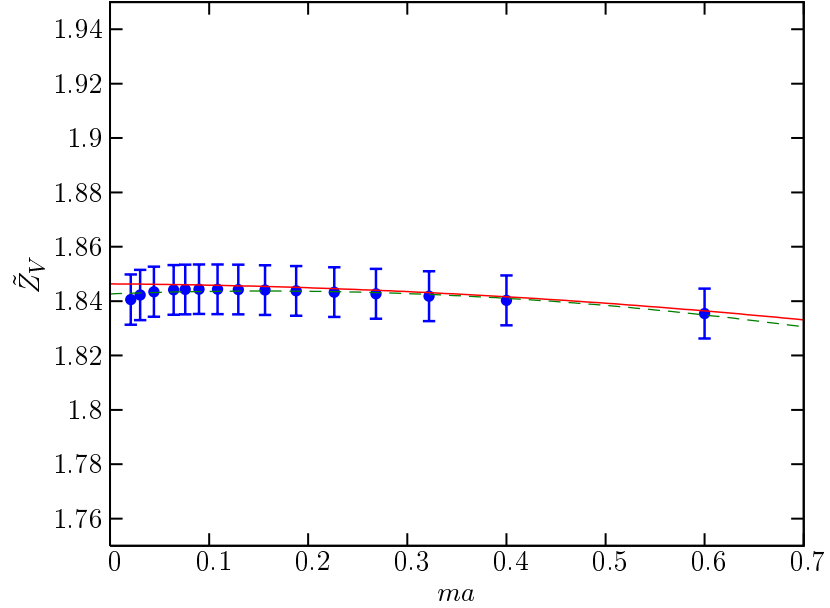


FIG. 16: The same as in Fig. 15 for $\tilde{Z}_V(ma)$.

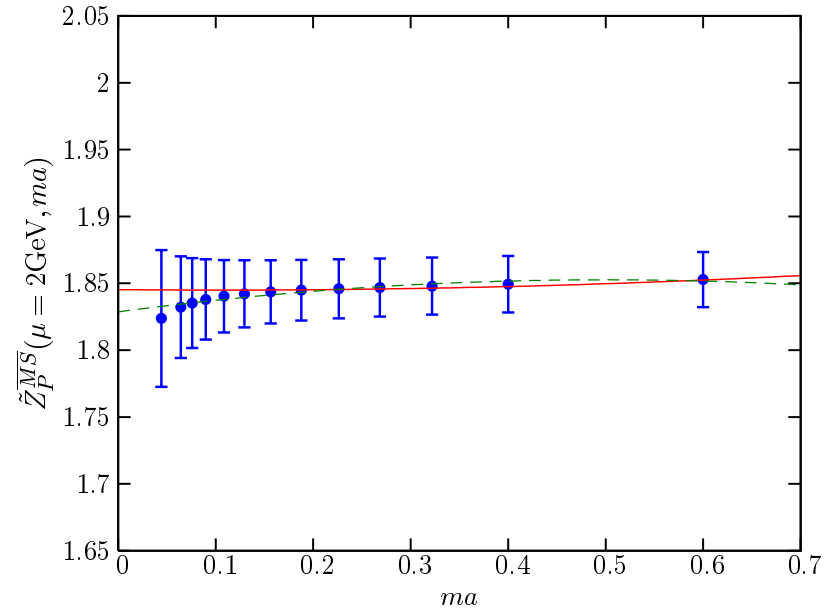


FIG. 17: The same as in Fig. 15 for the renormalization factor $\tilde{Z}_P^{\overline{\text{MS}}}(ma)$ in the $\overline{\text{MS}}$ scheme at $\mu = 2$ GeV.

$Z_A = Z_V$ due to chiral symmetry hold to high precision ($\sim 1\%$) for a large range of $(pa)^2$ with $(pa)^2 > 3$. The resultant check on the chiral symmetry relations are comparable to those of the domain-wall fermion [9] and somewhat better than the chirally improved fermion [10] where it is found that $Z_A/Z_V \sim 1.03$ and $Z_P/Z_S \sim 0.95$ for their smallest lattice spacing at

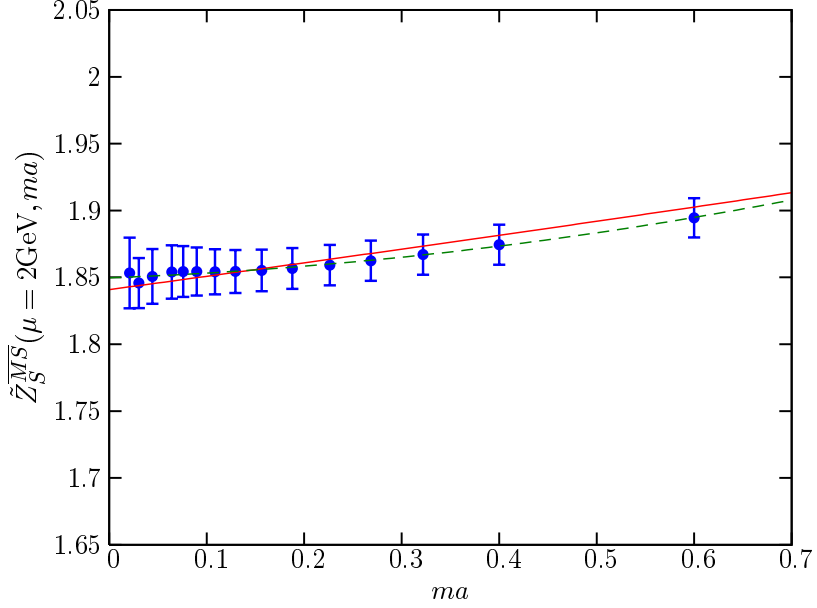


FIG. 18: The same as in Fig. 17 for $\tilde{Z}_S^{\overline{MS}}(ma)$.

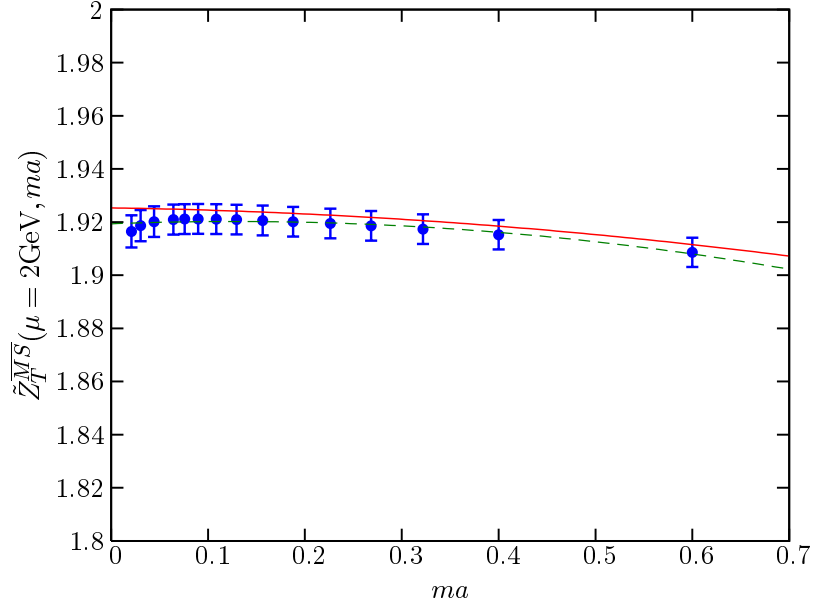


FIG. 19: The same as in Fig. 17 for $\tilde{Z}_T^{\overline{MS}}(ma)$.

$$a = 0.078 \text{ fm.}$$

We studied the finite ma errors in the renormalization of these composite operators. This is an important issue if one wants to use the same Dirac operator for both the light and heavy quarks. With present-day computers, it is not practical to reach a lattice spacing such that $ma \ll 1$ for the charm and bottom quarks. As such, one would like to have a Dirac operator

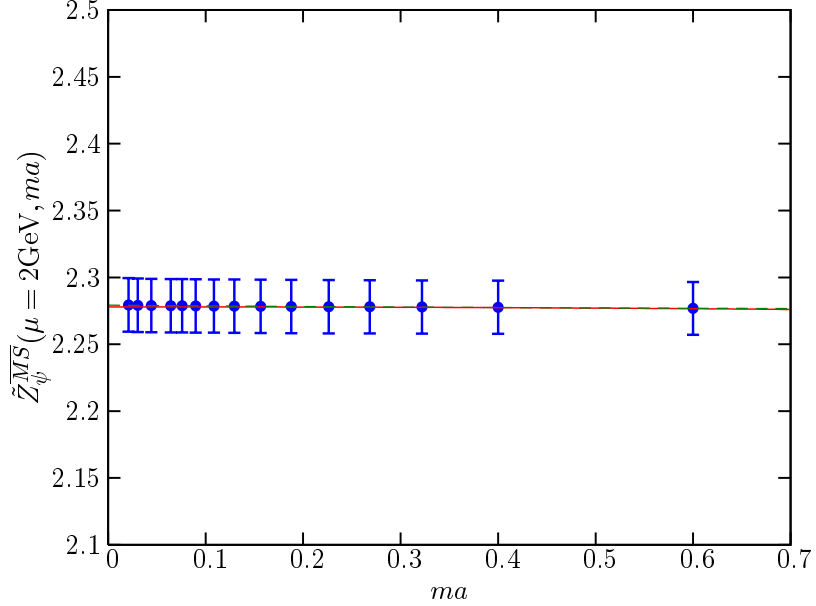


FIG. 20: The same as in Fig. 17 for $\tilde{Z}_\psi^{\overline{\text{MS}}}(ma)$.

which has chiral symmetry and, at the same time, has small $O(ma^2)$ and $O(m^2a^2)$ errors. It is suggested [16] that the overlap fermion with its effective quark propagator having the continuum form might be suitable for this purpose. Indeed the $O(ma^2)$ and $O(m^2a^2)$ errors in the dispersion relation and $\tilde{Z}_A(ma)$ are shown to be small [16]. In this study, we find that the finite ma corrections are also small in $\tilde{Z}_\psi(ma)$, $\tilde{Z}_V(ma)$, $\tilde{Z}_P(ma)$, $\tilde{Z}_S(ma)$, and $\tilde{Z}_T(ma)$. For ma as large as 0.6, the corrections are generally less than 3.5% in these renormalization factors we studied.

Since the lattice community is geared to carrying out large scale dynamical fermion calculations with chiral fermions, it is worth studying the $(pa)^2$ errors in the scale invariant vertices and the $(ma)^2$ corrections of the renormalization factors to gauge the $O(a^2)$ errors with different approximations and implementations of the overlap operator.

VIII. ACKNOWLEDGMENT

Support for this research from the Australian Research Council and DOE Grants DE-FG05-84ER40154 and DE-FG02-02ER45967 are gratefully acknowledged.

[1] G. Martinelli, C. Pittori, C.T. Sachrajda, M. Testa and A. Vladikas, Nucl. Phys. **B445**, 81 (1995).

[2] M. Ciuchini, E. Franco, G. Martinelli, L. Reina, L. Silvestrini, Z. Phys. **C68**, 239 (1995).

[3] G. Martinelli, S. Petrarca, C.T. Sachrajda and A. Vladikas, Phys. Lett. **B311**, 241 (1993); E: **B317**, 660 (1993).

[4] V. Gimenez, L. Giusti, F. Rapuano, M. Talevi, Nucl. Phys. **B531**, 429 (1998).

[5] A. Donini, V. Gimenez, G. Martinelli, M. Talevi and A. Vladikas, Eur. Phys. J. **C10**, 121 (1999).

[6] L. Giusti, V. Gimenez, F. Rapuano, M. Talevi and A. Vladikas, Nucl. Phys. (Proc. Suppl.) **B73**, 210 (1999).

[7] D. Becirevic *et al.*, Phys. Lett. **B444**, 401 (1998).

[8] JLQCD Collaboration, S. Aoki *et al.*, Nucl. Phys. (Proc. Suppl.) **B73**, 279 (1999).

[9] T. Blum, N. Christ, C. Cristian, C. Dawson, G. Fleming, G. Liu, R. Mawhinney, A. Soni, P. Vranas, M. Wingate, L. Wu, and Y. Zhestkov, Phys. Rev. **D66**, 014504 (2002).

[10] C. Gattringer, M. Göckeler, P. Huber, and C. B. Lang, hep-lat/0404006.

[11] L. Giusti, C. Hoelbling, C. Rebbi, Phys. Rev. **D64**, 114508 (2001); Erratum-ibid. **D65**, 079903,(2002).

[12] R. Narayanan, H. Neuberger, Phys. Lett. **B302**, 62 (1993); Nucl. Phys. **B443**, 305 (1995).

[13] H. Neuberger, Phys. Lett. **B417**, 141 (1998); Phys. Lett. **B427**, 353 (1998).

[14] M. Lüscher, Phys. Lett. **B428**, 342 (1998).

[15] R. G. Edwards, U. M. Heller, and R. Narayanan, Phys. Rev. **D59**, 094510 (1999).

[16] K.F. Liu and S.J. Dong, to appear in Int. Jour. Mod. Phys. A, hep-lat/0206002.

[17] H. Neuberger, Nucl. Phys. (Proc. Suppl.) **B83**, 67 (2000).

[18] S. J. Dong, F. X. Lee, K. F. Liu, and J. B. Zhang, Phys. Rev. Lett. **85**, 5051 (2000).

[19] E. Franco and V. Lubicz, Nucl. Phys. **B531**, 641 (1998)

- [20] S.J. Dong, T. Draper, I. Horváth, F.X. Lee, K.F. Liu, and J.B. Zhang, Phys. Rev. **D65**, 054507 (2002).
- [21] P. H. Ginsparg, K. G. Wilson, Phys. Rev. **D25**, 2649 (1982).
- [22] P. Hasenfratz *et al.*, Nucl. Phys. **B643**, 280 (2002), hep-lat/0205010.
- [23] Y. Kikukawa and A. Yamada, Nucl. Phys. **B547**, 413 (1999).
- [24] T.W. Chiu and S. Zenkin, Phys. Rev. **D59**, 074501 (1998).
- [25] H. Neuberger, Phys. Rev. **D57**, 5417 (1998).
- [26] T. W. Chiu, Phys. Rev. **D60**, 034503 (1999).
- [27] S. Capitani, M. Goeckeler, R. Horsley, P. E. L. Rakow, and G. Schierholz, Phys. Lett. **B468**, 150 (1999).
- [28] F. D. R. Bonnet, P. O. Bowman, D. B. Leinweber, A. G. Williams and J. B. Zhang, Phys. Rev. **D65**, 114503 (2002).
- [29] Y. Chen, S. J. Dong, T. Draper, I. Horváth, F. X. Lee, K. F. Liu, N. Mathur, and J. B. Zhang, Phys. Rev. **D70**, 034502 (2004).
- [30] A. Cucchieri and T. Mendes, Phys. Rev. **D57**, 3822 (1998).
- [31] F. D. R. Bonnet, P. O. Bowman, D. B. Leinweber, A. G. Williams and D. G. Richards, Austral J. Phys. **52**, 939 (1999).
- [32] J. van den Eshof *et al.*, Comput. Phys. Commun. **146**, 203-224 (2002); Nucl. Phys. (Proc. Suppl.) **106**, 1070-1072 (2002).
- [33] M. Bochicchio, L. Maiani, G. Martinelli, G.C. Rossi and M. Testa, Nucl. Phys. **B262**, 331 (1985).
- [34] P. Hassenfratz, Nucl. Phys. **B525**, 401 (1998).
- [35] C. Alexandrou, E. Follana, H. Panagopoulos, E. Vicari, Nucl. Phys. **B580**, 394 (2000).
- [36] K. Lane, Phys. Rev. **D10**, 2605 (1974); H.D. Politzer, Nucl. Phys. **B117**, 397 (1976); P. Pasqual and E. de Rafael, Z. Phys. **C12**, 127 (1982).
- [37] D. Becirevic, V. Gimenez, V. Lubicz, and G. Martinelli, Phys. Rev. **D61**, 114507 (2000).
- [38] S. Sharpe, Phys. Rev. **D46**, 3146 (1992).
- [39] N. Mathur, Y. Chen, S.J. Dong, T. Draper, I. Horváth, F.X. Lee, K.F. Liu, and J.B. Zhang, Phys. Lett. **B605**, 137 (2005).
- [40] K. G. Chetyrkin and A. Retey, Nucl. Phys. **B583**, 3 (2000).
- [41] J. A. Gracey, Nucl. Phys. **B667**, 242 (2003).

- [42] Aleksey I. Alekseev, Few Body Syst. **32**, 193 (2003).
- [43] T. van Ritbergen, J.A.M. Vermaseren and S.A. Larin, Phys. Lett. **B400** (1997) 379.
- [44] S. Capitani, M.Luscher, R. Sommer and H. Wittig, (ALPHA), Nucl. Phys. **B544**, 669 (1999),
- [45] J.B. Zhang, D.B. Leinweber, K.F. Liu, and A.G. Williams, Nucl. Phys. (Proc. Suppl.) **128**, 240 (2003), [arXiv:hep-lat/0311030].
- [46] R.C. Brower, H. Neff, and K. Orginos, hep-lat/0409118.
- [47] J. A. Gracey, Nucl. Phys. **B662**, 247 (2003).
- [48] Note that since we use the overlap fermion formalism, the fermion field ψ in Eqs. (4) and (6) will be replaced by $\hat{\psi} = (1 - D/2)\psi$, where D is the massless overlap operator. As a result, the $S(x, 0)$ and $S(0, y)$ are effective quark propagators to be described in Sec. III.